



A Review of Recent Progress in Fabrication Methods and Applications of Polydimethylsiloxane Sponge

Seungwoo Hong, Haeji Kim, Nadeem Qaiser, Peter Baumli & Byungil Hwang

To cite this article: Seungwoo Hong, Haeji Kim, Nadeem Qaiser, Peter Baumli & Byungil Hwang (2023) A Review of Recent Progress in Fabrication Methods and Applications of Polydimethylsiloxane Sponge, Journal of Natural Fibers, 20:2, 2264497, DOI: [10.1080/15440478.2023.2264497](https://doi.org/10.1080/15440478.2023.2264497)

To link to this article: <https://doi.org/10.1080/15440478.2023.2264497>



© 2023 The Author(s). Published with license by Taylor & Francis Group, LLC.



Published online: 03 Oct 2023.



Submit your article to this journal [↗](#)



Article views: 280



View related articles [↗](#)



View Crossmark data [↗](#)

A Review of Recent Progress in Fabrication Methods and Applications of Polydimethylsiloxane Sponge

Seungwoo Hong^a, Haeji Kim^a, Nadeem Qaiser^b, Peter Baumli^c, and Byungil Hwang^a

^aSchool of Integrative Engineering, Chung-Ang University, Seoul, Republic of Korea; ^bMaterial Science and Engineering, Physical Science and Engineering Division, 4700 King Abdullah University of Science and Technology (KAUST), Thuwal, Saudi Arabia; ^cInstitute of Physical Metallurgy, Metal Forming and Nanotechnology, University of Miskolc, Miskolc, Hungary

ABSTRACT

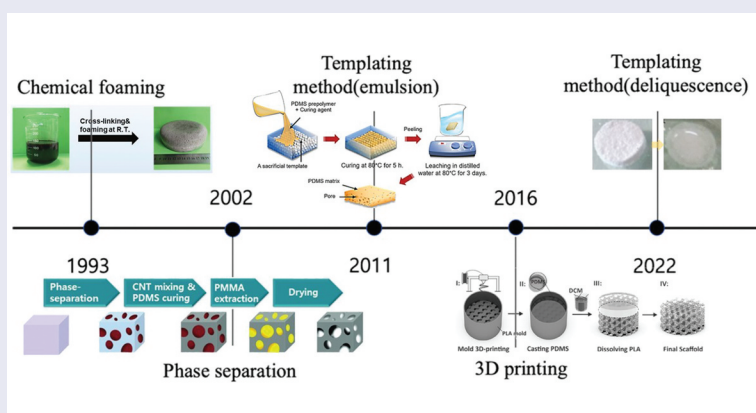
Research on stretchable materials has gained momentum with the increasing commercialization of wearable and flexible devices. Among the materials used in stretchable electronics, polydimethylsiloxane (PDMS) is popular owing to its remarkable mechanical properties when subjected to deformation. Recent studies have shown that sponge-like porous PDMS is gaining attention, as it provides high surface area and strong absorption properties as well as facilitates mass transfer, making it ideal for use in electronics. This review primarily focuses on the production method and application of porous PDMS. The article describes the various processing methods used to produce porous PDMS, including 3D printing, gas foaming, and phase separation, each of which results in different characteristics. Thus, researchers can choose the most suitable method according to their desired application. Porous PDMS provides channels for mass transfer and strong absorption properties that enable addition of fillers such as carbon nanotubes (CNTs), graphene, and metal nanoparticles, which can further enhance the functionality of the material. In addition, the review covers applications according to the filler used, such as sensors using CNT, flexible electrodes using NiO/MnO₂/CNT, and nanogenerators using ZnO. Choosing the right material for the filler is important for obtaining the desired characteristics as per its application.



KEYWORDS

Polydimethylsiloxane; porous PDMS; PDMS sponge; stretchable electronics; fabrication methods; wearable

关键词

聚二甲基硅氧烷; 多孔 PDMS; PDMS海绵; 可拉伸电子产品; 制造方法; 可穿戴的



CONTACT Byungil Hwang  bihwang@cau.ac.kr  School of Integrative Engineering, Chung-Ang University, Seoul 6974, Republic of Korea

© 2023 The Author(s). Published with license by Taylor & Francis Group, LLC.

This is an Open Access article distributed under the terms of the Creative Commons Attribution-NonCommercial License (<http://creativecommons.org/licenses/by-nc/4.0/>), which permits unrestricted non-commercial use, distribution, and reproduction in any medium, provided the original work is properly cited. The terms on which this article has been published allow the posting of the Accepted Manuscript in a repository by the author(s) or with their consent.

摘要

随着可穿戴和柔性设备的日益商业化,可拉伸材料的研究势头越来越大.在可拉伸电子产品中使用的材料中,聚二甲基硅氧烷(PDMS)因其在变形时具有显著的机械性能而广受欢迎.最近的研究表明,海绵状多孔PDMS正受到关注,因为它提供了高表面积和强吸收性能,并促进了传质,使其成为电子产品的理想用途.本文主要对多孔PDMS的制备方法及应用进行综述.文章描述了用于生产多孔PDMS的各种加工方法,包括3D打印、气体发泡和相分离,每种方法都会产生不同的特性.因此,研究人员可以根据他们想要的应用选择最合适的方法.多孔PDMS提供了传质通道和强吸收性能,能够添加填料,如碳纳米管(CNTs)、石墨烯和金属纳米颗粒,这可以进一步增强材料的功能.此外,该综述涵盖了根据所用填料的应用,例如使用CNT的传感器、使用NiO/MnO₂/CNT的柔性电极和使用ZnO的纳米发生器.为填料选择合适的材料对于根据其应用获得所需的特性非常重要.

1. Introduction

With the development of wearable devices, the importance of flexible electronics is emerging (Butt, Kazanskiy, and Khonina 2022; Ha et al. 2022; Seo et al. 2022; Kim et al. 2023). In electronic devices such as displays, solar cells, and energy-storage elements such as batteries, components such as active layers and electrodes play an important role (Szalai et al. 2022; Ha et al. n.d.). For flexible electronics in particular, the above mentioned components must be deformed without degradation of electronic properties; for this purpose, polymer substrates are used (Hwang, Han, and Matteini 2022; Kim et al. 2019; Lee, Kim, and Hwang 2019; Hwang et al. 2022). Examples of materials used in polymer substrates include poly(3,4-ethylenedioxythiophene):poly(styrenesulfonate)(PEDOT:PSS), polyethylene terephthalate(PET) (Faraj, Ibrahim, and Ali 2011), polyethylene naphthalate(PEN), and polydimethylsiloxane(PDMS). Among them, PDMS is the most suitable material that is frequently used in engineering applications such as wearables biomedical devices, displays, and sensors (Cui et al. 2016; Ha et al. 2023) owing to its excellent optical properties (Kim, Koo Kim, and Chan Jeong 2011), wide thermal stability and mechanical reliability (Cao et al. 2020; Zhang et al. 2021).

Moreover, recent research has been actively focused on manufacturing PDMS in the form of a porous structure and applying it to electronics (Dan et al. 2019; Pan et al. 2020; Yu et al. 2017). Because PDMS has a sponge-type structure, its mechanical properties can be improved compared to that of bulk PDMS by adjusting the pore characteristics (Tan and Zheng 2022). For instance, it was confirmed that the smaller the pore size distribution, the stronger is the stiffness. Moreover, if the pore is small, the materials can withstand a larger strain (Abshirini et al. 2021). In other words, the smaller the pore size, the more deformation it can withstand, which is a great advantage when applied to flexible and stretchable electronics. In addition, because of its porous structure, PDMS sponge has a higher surface area than typical bulk PDMS, showing higher absorption performance (Lu et al. 2018; Zhang et al. 2019). This maximizes the performance of nanocomposite porous PDMS by wetting fillers well in a large area between pores. For example, excellent mechanical and electrical properties can be obtained by coating PDMS with fillers such as CNTs and metal nanowires. By utilizing the advantages of PDMS and fillers mentioned above, porous PDMS is used in various applications. The flexibility of PDMS and the electrical properties improved through the fillers are adopted in flexible sensors (Kim, Jang, and Je Hoon 2019; He et al. 2021; Herren et al. 2021; Jung et al. 2019, 2020; Luo et al. 2019; Sun et al. 2019), nanogenerators (He et al. 2016; Tantraviwat et al. 2020), supercapacitors (Kim, Qaiser, and Hwang 2023; Shieh et al. 2017; Song et al. 2017), and fire shielding (Cao et al. 2020; Guo et al. 2022; Lv et al. 2022; Zhang et al. 2021). In addition, the high surface area of the porous structure and the hydrophobic behavior of PDMS is used for oil/water separation (Ozkan et al. 2023; Yu et al. 2017). Moreover, the porous PDMS nanocomposites decorated with MXene/cellulose nanofiber by silane

surface modification shows unique multifunctional properties for various applications (Chen et al.). Furthermore, PDMS sponge shows high thermal stability owing to the Si – O–Si backbone structure and air, which is attributable to its porous structure (Du et al. 2021). Therefore, PDMS is used in many fields as a thermally insulating material. In addition, the fabrication can be performed in various ways such as phase separation (Abshirini et al. 2020), 3D printing (Montazerian et al. 2019; Woo et al. 2021), direct templating (salt/sugar leaching, colloidal crystals, and nickel foam) (Turco et al. 2017; Yu et al. 2017), and gas foaming (Cao et al. 2020; Guo et al. 2022; Han et al. 2023; Hu et al. 2022; Zhang et al. 2021). Because parameters such as pore size, pore distribution, and pore shape obtained in each process are different, selecting the appropriate processing method is important.

In the pursuit of realizing flexible and wearable electronic devices in the future, porous PDMS materials with excellent mechanical strength and thermal stability (Guo et al. 2022) have been studied in depth recently. However, in the last five years, no review articles have been published in this regard. Our review introduces concrete and diverse aspects of PDMS sponge with theoretical support. Therefore, this paper, which deals with the latest studies on the fabrication and applications of porous PDMS, will be of great help to the readers in this wide field.

2. Methods to fabricate PDMS sponge

2.1. 3D printing

3D printing technology is currently being applied in various ways to medical care, fashion, and buildings. Complex structures can readily be made at low cost owing to low wastage of materials. Recently, a method of manufacturing a 3D porous PDMS with a 3D structure via 3D printing technology has been studied (Montazerian et al. 2019; Woo et al. 2021).

Montazerian et al (Montazerian et al. 2019) measured the mechanical property by creating a porous PDMS of a variable surface type using the 3D-printed private template method. They created a polylactic acid (PLA) mold with a 3D printing machine, where the mold shape was prepared in various ways through CAD modeling [Figure 1\(a\)](#). Scaffold structures based on TPMS surface-based architectures were designed. The explicit approximation of TPMS (Gandy et al. 2001) is given by the equation below:

$$\Gamma(r) = \sum_{l=1}^L \sum_{m=1}^M \mu_{lm} \cos(2\pi\kappa_1(P_m^T \cdot r)) = C, \quad (1)$$

where κ_1 = scale parameter, $P_m = [a_m, b_m, c_m]^T$ = basis vector that shows a basic plane in the 3-Space E^3 , μ_{lm} = periodic moment, and $r = [x, y, z]^T$ = location vector with homogeneous coordinates. In Equation 1, the left side represents a pore topology defined by a combination of sine and cosine. In this equation, three constants (C) are most known, namely, P-, D-, and G-surface geometries, and are correlated with porosity. Their equations are as follows (Gandy et al. 2001):

$$P - \text{Surface} : \cos(2\pi x) + \cos(2\pi y) + \cos(2\pi z) = C, \quad (2)$$

$$D - \text{Surface} : \cos(2\pi x) \cos(2\pi y) \cos(2\pi z) - \sin(2\pi x) \sin(2\pi y) \sin(2\pi z) = C, \quad (3)$$

$$G - \text{Surface} : \sin(2\pi x) \cos(2\pi y) + \sin(2\pi z) \cos(2\pi x) + \sin(2\pi y) \cos(2\pi z) = C. \quad (4)$$

After preparing molds of three shapes using Equation 1, PDMS samples were poured into each mold. Subsequently, the molds were immersed in dichloromethane (DCM). All the PLA molds were melted by DCM, and the residue was washed out for approximately 5 h to produce a PDMS sponge [Figure 2\(b\)](#). The optical image of the created PDMS sponge can be seen in [Figure 2\(c-f\)](#).

Unlike the abovementioned method, Woo et al (Woo et al. 2021) produced a porous PDMS without a separate etching process using the PDMS precursor direct ink writing method without making molds [Figure 3\(a\)](#). [Figure 3\(d\)](#) presents the stress – strain curve of nonporous and porous

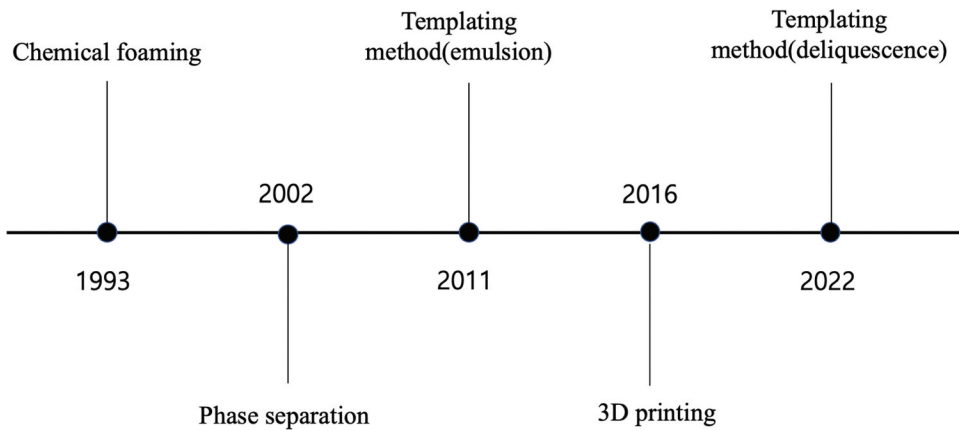


Figure 1. Timeline fixing the milestone research articles about the topic of the porous PDMS.

PDMS, which show that the porous structure is much superior in mechanical characteristics compared to a nonporous structure.

By using 3D printing technology, porous PDMS with excellent mechanical characteristics can be created. In addition, as the porous structure can be precisely made, the characteristics can be controlled according to the application (Zhu, Handschuh-Wang, and Zhou 2017). However, thus far, the high cost of equipment has been an issue (Oropallo and Piegl 2016; Zhu, Handschuh-Wang, and Zhou 2017). Moreover, it is unsuitable for mass production because the fabrication process is lengthy (Oropallo and Piegl 2016). Therefore, considerable research is required to resolve these issues.

2.2. Chemical foaming method

The chemical foaming method can overcome the above mentioned disadvantages of 3D printing (Oropallo and Piegl 2016; Zhu, Handschuh-Wang, and Zhou 2017). Because chemical foaming is an inexpensive and facile method, it has recently been actively investigated as a method for preparing porous sponges (Long et al. 2018).

Long et al (Long et al. 2018) prepared porous graphene/PDMS using the chemical foaming method. NH_4HCO_3 composition products leave little residue in the pore. In addition, as the particle size of NH_4HCO_3 is very small, it can be mixed evenly with PDMS and the loading of the powders can be controlled to control the porosity. The fabrication process for porous graphene/PDMS is as follows. First, PDMS elastomer and dimethylbenzene are mixed to ensure that graphene is well dispersed. Then, NH_4HCO_3 powder and curing agent are added to the mixture. Thereafter, dimethyl benzene is evacuated in vacuum to remove dimethyl benzene, put in a polytetrafluoroethylene mold, and then cured for 20 min [Figure 4\(a\)](#). The SEM image of the prepared graphene/PDMS is shown in [Figure 4\(c\)](#). Long et al. conducted a tensile test to measure the mechanical properties of the produced graphene/PDMS, which showed ~64% stretchability [Figure 4\(b\)](#). Finally, the resistance response according to the cycling of the tension strain sensor was measured [Figure 4\(d\)](#). The resistance response value at 1000 cycles changed only slightly, indicating its appreciable stability.

Cao et al (Cao et al. 2020). fabricated pure porous sponge, porous graphene oxide (GO)-PDMS, porous graphene oxide nanoribbon (GONR)-PDMS with the chemical foaming method using vinyl dimethicone (PDMS-Vi), dihydroxy PDMS (PDMS-OH), hydrogen dimethicone, and Pt as the catalyst. Porous GO-PDMS and porous GONR-PDMS were produced in the same way, and GO and GONR aqueous solutions were used instead of water as foaming agents [Figure 5\(a\)](#). In the case of pure porous PDMS, the size of most pores was measured as 500 μm or more. However, when 0.1% GO and GONR were mixed, the pore size was well distributed at 200–300 μm [Figure 5\(b-d\)](#).

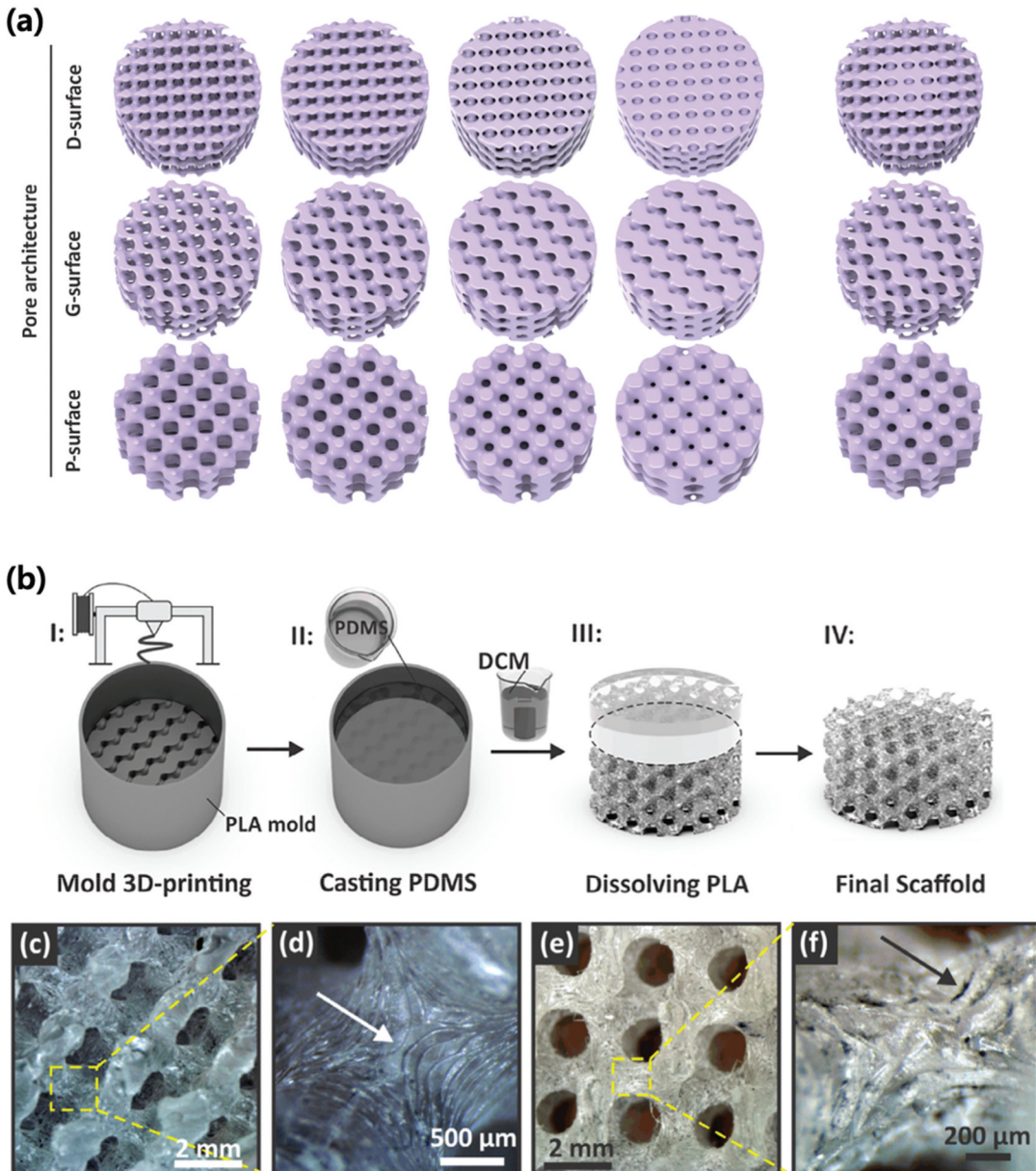


Figure 2. (a) schematic representation of the scaffold designs with different TPMS geometries with uniform and radially graded porosity. (b) fabrication process for the internally architected porous PDMS scaffolds. (c,d) optical images of a D-surface structure. (e,f) optical images of a G-surface structure (Montazerian et al. 2019). Reprinted with permission from (Montazerian et al. 2019); copyright 2019 Elsevier.

Cao et al. measured the compressive stress and strain of the prepared composites. When 60% strain was applied, the maximum stress of PDMS mixed with GO and GONR was higher than that of pure porous PDMS. In general, in each case, the higher the filler content, the higher is the maximum stress, which implies that the mechanical characteristics could be improved as much as necessary by adjusting the contents of GO and GONR. In fact, in the case of pure porous PDMS at 60% strain, a stress value of ~ 4.5 kPa was found. Porous GONR-PDMS showed a stress value of approximately 0–9.1 kPa, and porous GO-PDMS showed a stress value of around 11 kPa. This can

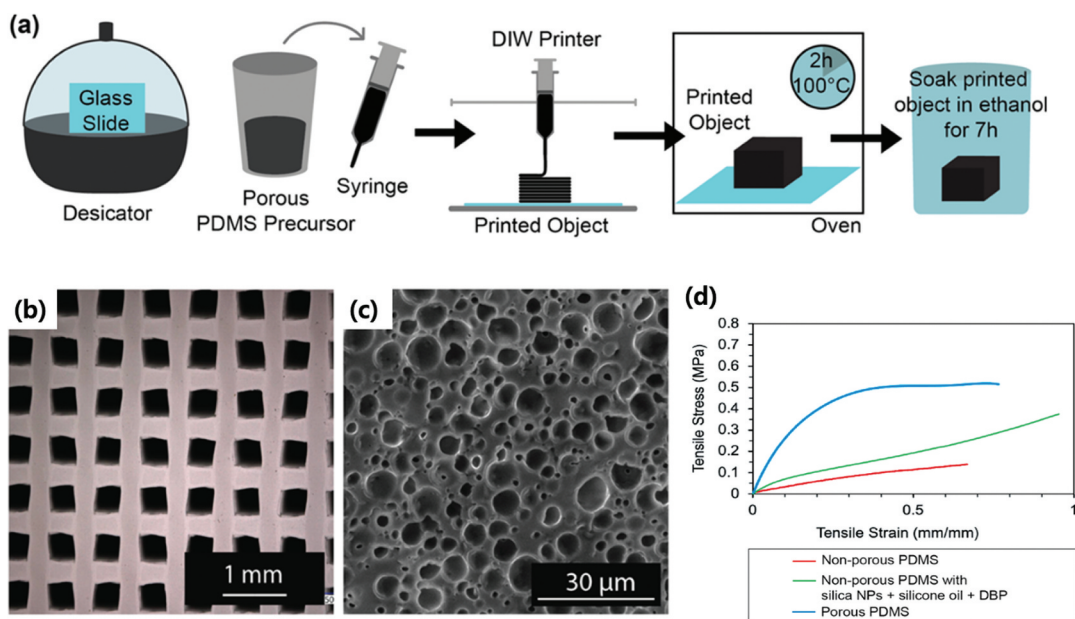


Figure 3. (a) step-by-step process of the preparation and printing of the porous PDMS precursor. (b) optical microscopy image of the lattice structure. (c) Cross-sectional scanning electron microscopy (SEM) image of porous PDMS without silica NPs. (d) stress – strain curves of nonporous PDMS (red), nonporous PDMS with silica NPs, silicone oil, and DBP (green), and porous PDMS (blue) with 0–100% infill density (Woo et al. 2021). Reprinted with permission from (Woo et al. 2021); copyright 2021 American Chemical Society.

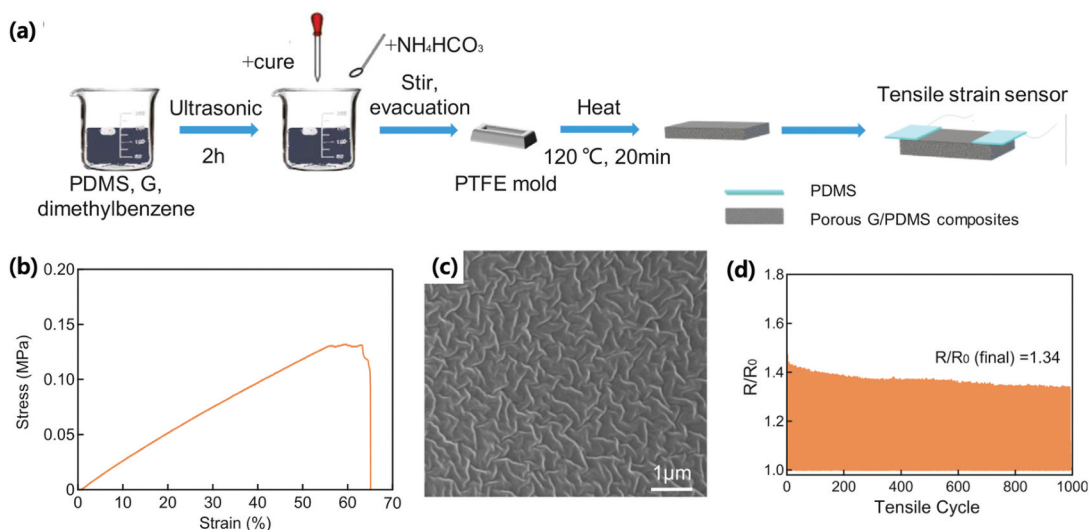


Figure 4. (a) schematic showing the preparation method for porous graphene/PDMS composites. (b) stress – strain curves of the porous graphene/PDMS composite under tensile test. (c) SEM image of the folding microstructure of the graphene/PDMS composite. (d) repeatability test (Long et al. 2018). Reprinted with permission from (Long et al. 2018); copyright 2018 Elsevier.

be seen as the formation of the GONR and GO layer on the skeleton surface, and the resulting change in the distribution of pore size affects the mechanical properties Figure 6(a,b).

As PDMS sponge is applied to various electronic devices (He et al. 2016, 2021; Jung et al. 2019; Song et al. 2017; Sun et al. 2019; Tantraviwat et al. 2020), controlling its characteristics such as

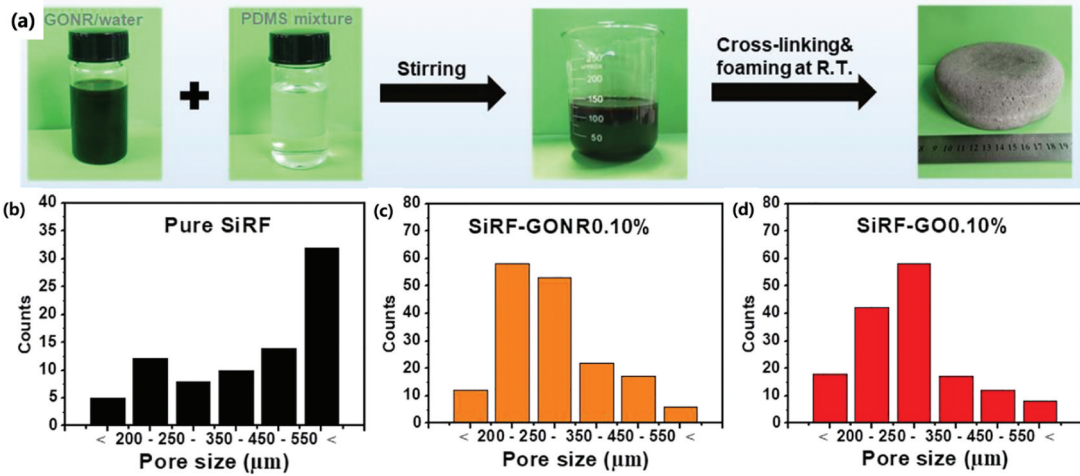


Figure 5. (a) digital images of the fabricating process of the GONR coated SiRF at ambient temperature. Pore size distribution of (b) pure SiRF, (c) SiRF-GONR 0.10%, (d) SiRF-GO 0.10% (Cao et al. 2020). Reprinted with permission from (Cao et al. 2020); copyright 2020 Elsevier.

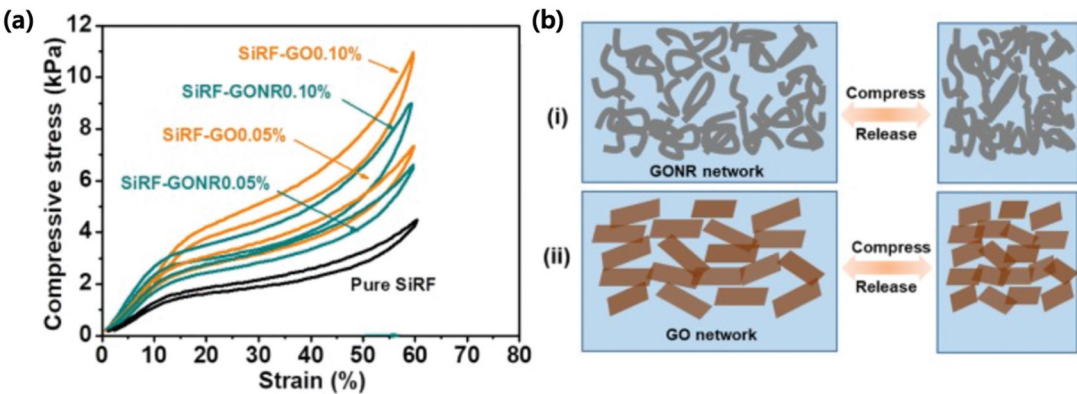


Figure 6. (a) compressive stress-strain curves at strain = 60% and (b) schematic of the structural evaluation during the compressive process. Reprinted with permission from (Cao et al. 2020); copyright 2020 Elsevier.

pore size and porosity is crucial. However, the chemical and gas foaming methods mentioned above have a major disadvantage in terms of the difficulty controlling the pore size (Zhu, Handschuh-Wang, and Zhou 2017).

2.3. Sacrificial templating method

The self-removing template method has the advantage of not requiring expensive equipment and taking less time (Keller et al. 2022; Pharino et al. 2021). It is also the most commonly used method because it is very effective in scale-up (Keller et al. 2022; Pharino et al. 2021; Zhou et al. 2021). The overall manufacturing process is as follows (Keller et al. 2022): Mix PDMS and curing agent (10:1) and add an appropriate amount of materials to be templated and stir. Then, put the mixture in an oven for curing, soak it in water, and then the capillary action dissolves sugar whose water is dispersed in the mixture to create a porous structure. A substance often used in this method is sugar or salt. This is because they are cheap, easy to obtain, and eco-friendly. In addition, as the solvent used is water, it is harmless, and the salt or sugar leached in water can be reused.

2.3.1. Templating method: water immersion

The water immersion method is a method of self-removing the template by immersing the PDMS sample in water. Keller et al (Keller et al. 2022) prepared a PDMS sponge using three types of materials: NaCl, brown sugar, and white sugar. The produced PDMS sample was immersed in water for 24 h, and the water-soluble substances, namely, sugar and NaCl, were removed to create a porous PDMS sponge. Pharino et al. also conducted an experiment using the water immersion method, but there was a slight difference in the conditions. The curing temperature and leaching time were different, and the process of degassing was added. The experiment was conducted using different types of commercial crystals: white sugar tube and monosodium glutamate(MSG). Viscous PDMS was manually stirred for 5 min, and degassing was performed in a vacuum desiccator for 1 h. Then, it was cured at 80°C for 5 h and leached at 80°C in distilled water for 3 d. Water was changed every hour to ensure templating, and after the leaching process, a drying process was performed in an oven at 100°C for 1 d to obtain a PDMS sponge (Figure 7).

2.3.2. Templating method: deliquescence method

The deliquescence method is a method of continuously templating materials that have the property of deliquescence by leaving them at room temperature. This method is also one of the most widely used methods because it is cheap and does not require any equipment (Keller et al. 2022). Keller et al. fabricated PDMS samples with LiCl and $CaCl_2$ using the deliquescence property. Templating was performed by exposure for 1 week under the conditions of open air at 21°C and 45% humidity (Figure 8).

Keller et al. measured the tensile stress, observing values ranging from 80 to 310 KPa. This result indicates that the PDMS sponge prepared by the template method has excellent mechanical properties. The pore diameter was the largest with an MSG of $\sim 1007 \mu\text{m}$, followed by brown sugar. NaCl based on dimethicone and LiCl showed the lowest results between 150 and 300 μm . The contact angle associated with hydrophobicity was as low as 116° in the PDMS sponge using a white sugar tube as a material and was intermediate in white sugar crystal, msg, and NaCl (between 120° and 130°).

Zhou et al (Zhou et al. 2021) prepared a PDMS sponge through the water immersion method by mixing granulated crystal sugar particles (100–600 μm) and sugar powder ($\sim 10 \mu\text{m}$). Sugar powder and PDMS mixture were put in a mold and allowed to cure for 8 h. Then, sugar was dissolved in a water bath at 60°C and air-dried at 80°C. Here, Zhou et al. conducted an experiment with different

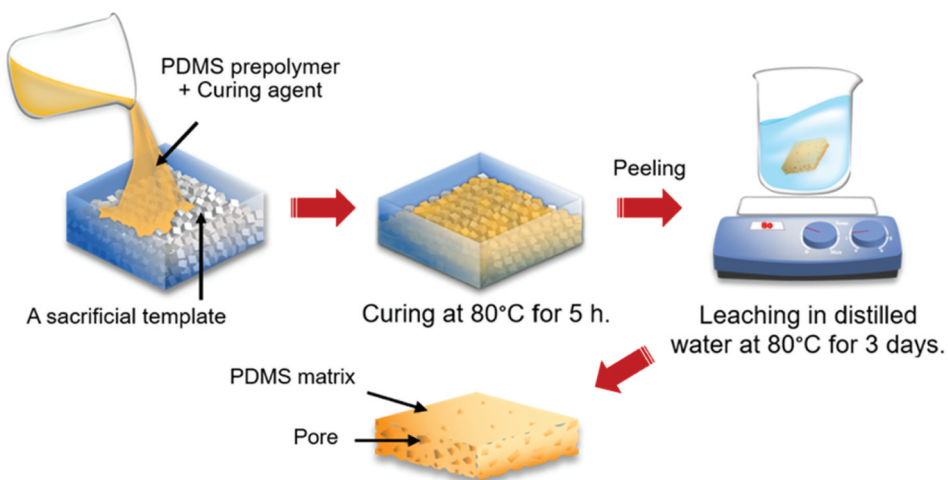


Figure 7. Schematic illustration of PDMS sponge preparation. The PDMS polymer and curing agent were mixed to a weight ratio of 10:1. Viscous PDMS was then added to the mold and curing at 80°C for 5 h. finally leaching in distilled water at 80°C for 3 days (Pharino et al. 2021). Reprinted with permission from (Pharino et al. 2021); copyright 2021 Elsevier.

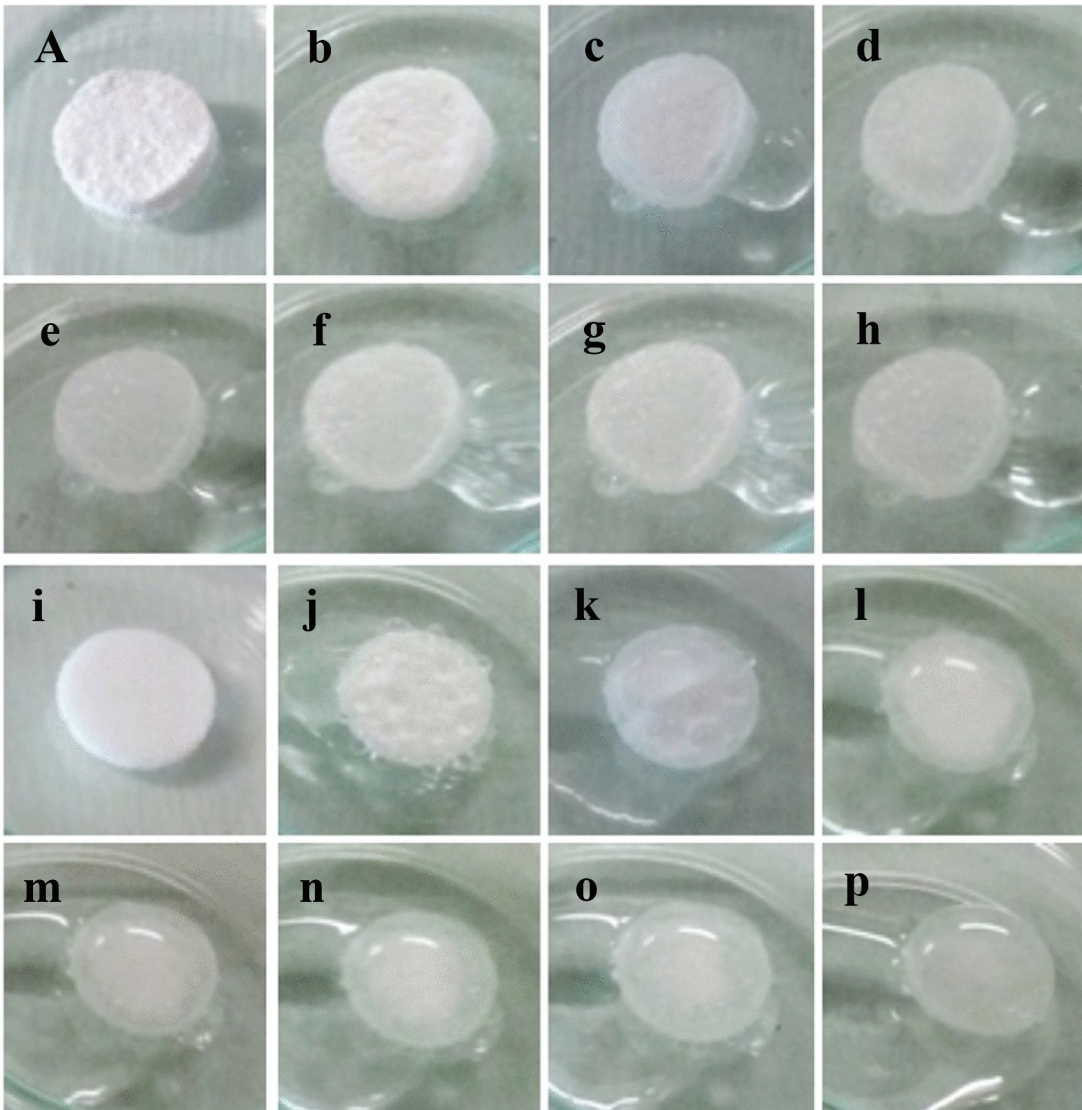


Figure 8. Images of the self-removing deliquescence process. (a, i) PDMS sponges prepared with CaCl₂ and LiCl respectively. (b-h), (j-p) expulsion of salt solution within the PDMS sponges as the CaCl₂/LiCl hard templates are solubilized via deliquescence at 1, 2, 3, 4, 5, 6, and 7 d (Keller et al. 2022). Reprinted with permission from (Keller et al. 2022); copyright 2022 Springer nature Switzerland AG. Part of Springer nature.

ratios of PDMS and sugar (1:2, 1:5, and 1:10). The pore size distributions were measured from SEM images of the sample; they are shown in Figure 9(a). When the mixing ratio was 2:1, the pore size was the smallest, and it could be verified that a peak appeared at 0–300 μm . Further, two peaks existed at 100 and 1600 μm when the mixing ratio was 5:1 Figure 9(b,c).

2.4. Phase separation

The phase separation method is the most reliable technology for manufacturing porous polymers, and unlike other methods, the pore size achievable with this method is not limited to template size (Ulbricht 2006). Templating materials do not need to be removed and are surfactant-free techniques.

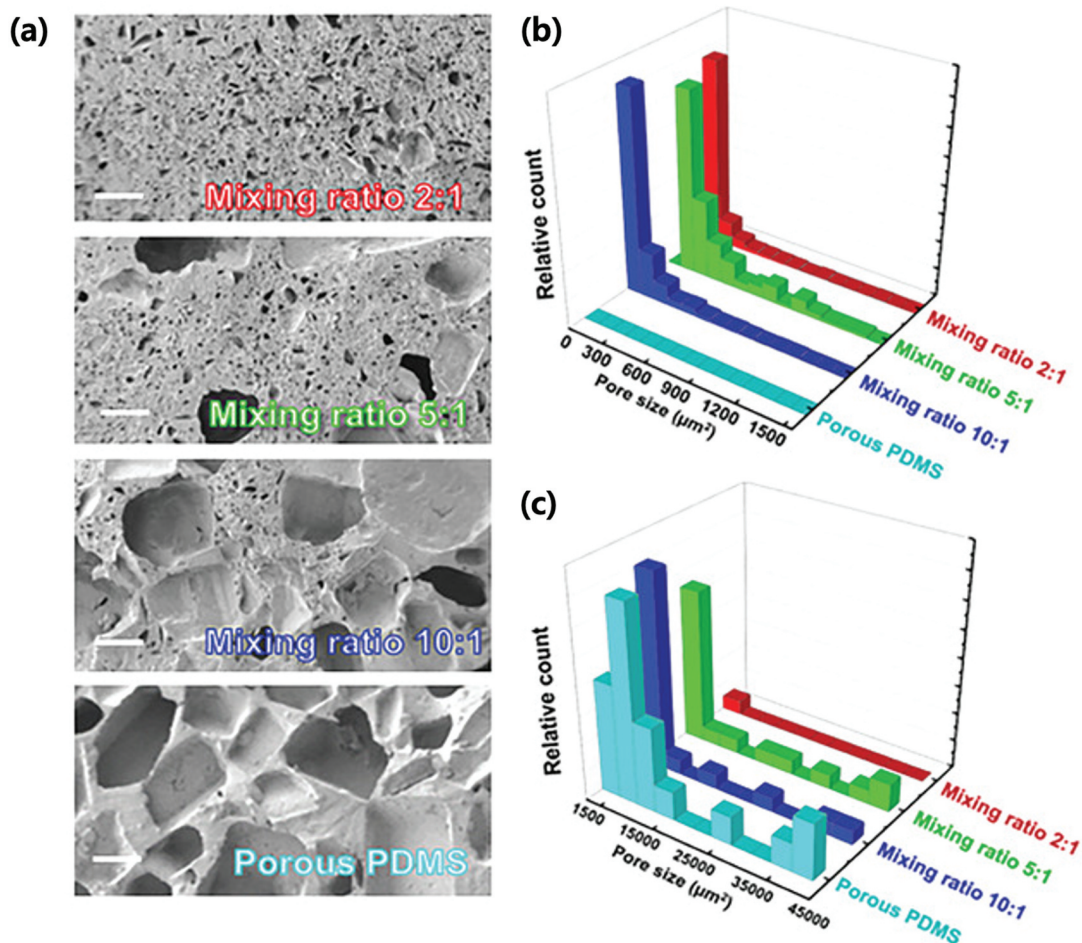


Figure 9. (a) SEM images of four porous PDMS samples with different pore distributions. The scale bar in the SEM images is 150 μm . (b,c) extracted pore size distributions from (a) (Zhou et al. 2021). Reprinted with permission from (Zhou et al. 2021) ; copyright 2021 John Wiley and sons.

Therefore, it is not necessary to consider the adverse impact due to the surfactant (Abshirini et al. 2021). Because of these advantages, despite the complexity compared to the sacrificial template, the phase separation method has been extensively studied recently (Wang et al. 2021).

Abshirini et al (Abshirini et al. 2020) produced porous PDMS using the phase separation method with this mechanism. Water and PDMS base elastomer were mixed, and tetrahydrofuran (THF) was added. The mixture was stirred until the solution became a viscous mixture; then, a cooling agent was added before molding, and the resultant mixture was mixed with a mechanical shear mixer for 20 min. Porous PDMS was fabricated by pouring the completed polymer solution into a mold and heat-treating it at various temperatures for solvent evaporation, polymer curing, and nonsolvent phase removal Figure 10(a). The concentration of PDMS was fixed at 40 wt%, and a sample was prepared by changing the ratio of water to THF (α) from 1 to 8. SEM images and pore distribution of the prepared samples can be confirmed in Figure 10(b-g). With a reduction in the value of α (water/THF ratio), the pore size showed a general tendency to increase.

The elastic modulus obtained from the stress – strain curve was 0.49 MPa for $\alpha = 1$ and 1.05 MPa for $\alpha = 8$ (Figure 10(h)). As the α value increased, the modulus value also increased. For a more accurate comparison, the strain value at a stress of 0.18 MPa is shown in Figure 10(i). The lower the

water/THF ratio (α), that is, the larger the pore size, the higher is the deformation observed. This result confirms that the desired mechanical properties could be obtained by adjusting the α (solvent/nonsolvent ratio) value associated with the pore size.

In another study, Abshirini et al (Abshirini et al. 2021) produced porous PDMS by employing the two-step phase separation method using toluene in addition to THF. The overall manufacturing process was the same as previously Abshirini et al (Abshirini et al. 2021) used, with the difference being that toluene and THF were mixed in different mixing ratios and used as solvent phases. Because of the difference in the boiling point between the two materials, THF and toluene were evaporated in two steps at once. By using this point, the pore size and distribution were controlled by adjusting the heat treatment procedure. Several samples were prepared with different THF/solvent ratios, and SEM images were taken (Figure 11). Two separate pore size distributions were obtained. A pore with an average size of 28 μm was created by the THF effect, the first step of phase separation, and a pore with an average size of 509 μm was created by the evaporation of toluene. This means that the porous network changes according to the THF/toluene ratio, which results in different pore morphologies and mechanical properties.

The researchers calculated the relative area fragments of the large pores for several samples according to the following equation:

$$\rho_L = 100 \frac{A_L}{A_L + A_S}, \rho_s = 100 \frac{A_s}{A_L + A_s}. \quad (5)$$

The ρ_L value according to the THF/solvent ratio can be confirmed from the graph in Figure 12(a), and the porosity according to the ρ_L value (0%, 30%, 54%, 86%, and 100%) is presented in Figure 12(b). Figure 12(b) reveals that the porosity is close to 60% for any ρ_L value. The THF/solvent ratio does not affect the porosity, which depends only on the polymer concentration. In other words, the pore size can be adjusted by adjusting the amount of THF and toluene, but the total volume fraction is the same. Figure 12(c) shows the stress – strain curve up to the failure point for each sample. The modulus value at $\rho_L = 54\%$ calculated from the stress – strain curve is 0.64 MPa, and the modulus value at ρ_L is 0.95 MPa. Compared to 1.83 MPa, which is the modulus value of a general solid sample, the modulus value in the case of porosity is lower, which implies that the porous structure results in a flexibility characteristic. In addition, the strain value at the failure point of the sample varies depending on the porosity degree, that is, the ρ_L value. This means that the value of flexibility may be adjusted through the adjustment of the THF/solvent ratio. Unlike the template method, applying the phase separation method to fields such as green chemistry and oil separation is difficult because organic solvents such as toluene are used in experiments (Zhu, Handschuh-Wang, and Zhou 2017). However, it has the advantage of being able to be scaled up because controlling the pore size is possible and the fabrication process is simpler than the template method (Abshirini et al. 2020, 2021).

Lee et al (Lee et al. 2012) also produced porous CNT/PDMS in a phase separation method Figure 13(a). To control the size of the pore, a sample was produced by changing the ratio of PDMS:PMMA; the ratio of block copolymers (PDMS-b-PMMA) was also adjusted, and the pore dimension of the sample obtained from the SEM image of Figure 13(b-i) can be checked, and the values are summarized in Table 1.

Lee et al. measured the mechanical properties of the created sample. Young's modulus was higher when PDMS:PMMA was 8:2 than when PDMS:PMMA was 7:3. The high mechanical stiffness of the 8:2 sample was due to the small pore volume fracture and small pore size. The maximum strain also showed different values depending on the PDMS:PMMA ratio, and as the ratio of block copolymers increased, that is, as the size of the pore decreased, the fracture strain increased in the 7:3 sample. However, for a ratio of 8:2, the fracture strength and strain tended to decrease as the fraction of the block copolymer increased. Detailed values and graphs are summarized in Figure 13(j-l) and Table 1.

Unlike the template method, applying the phase separation method to fields such as green chemistry and oil separation is difficult because organic solvents such as toluene are used in

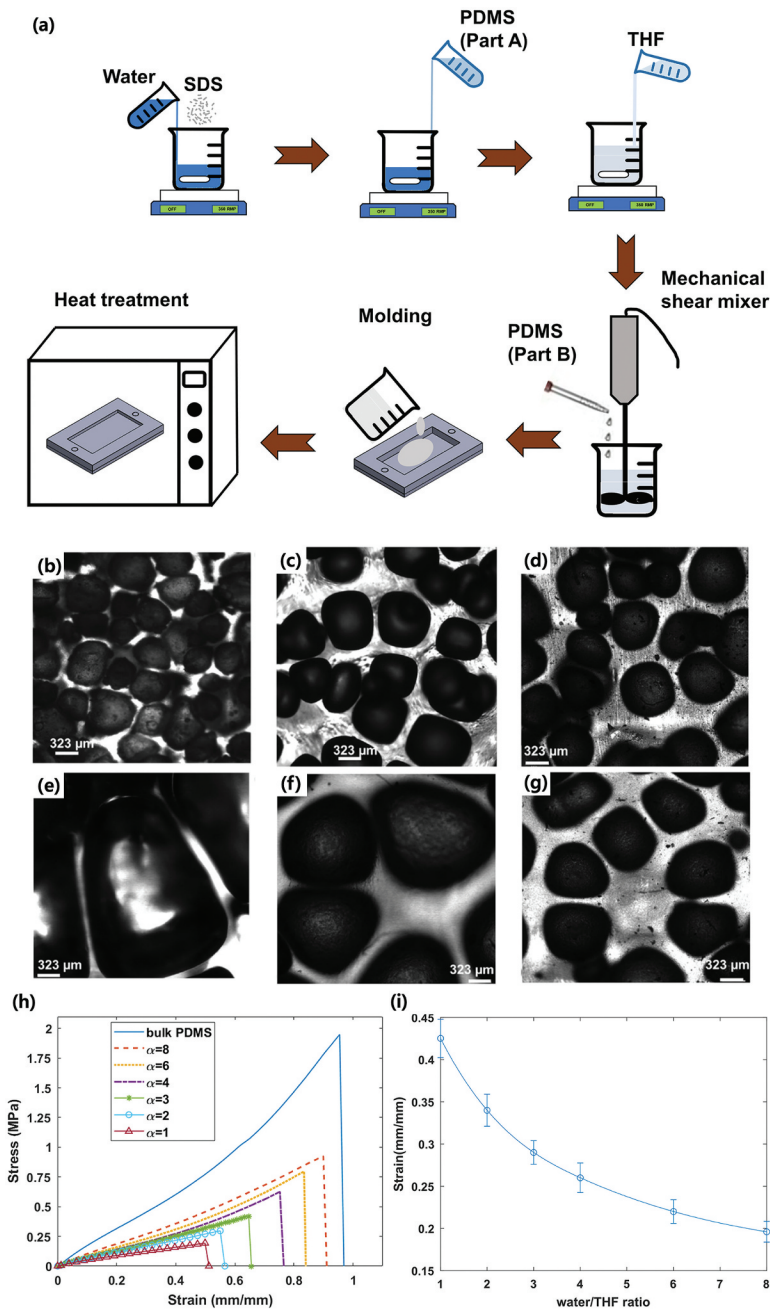


Figure 10. (a) schematic showing the preparation of polymer solution and molding. PDMS, polydimethylsiloxane; THF, tetrahydrofuran. Water was mixed with the PDMS elastomer at 1000 RPM. And then, THF was added to PDMS. After blending the solution, add the curing agent and put it into the customized mold. Finally, heat treatment is performed to obtain a sample. Microscope images showing the pore distribution for the samples with 40% PDMS and b) $\alpha = 8$, c) $\alpha = 6$, d) $\alpha = 4$, e) $\alpha = 3$, f) $\alpha = 2$, and g) $\alpha = 1$. h) stress – strain curve for samples with different α at 40% PDMS concentration. i) strain of the samples with 40% PDMS at a stress of 0.18 MPa (Abshirini et al. 2021). Reprinted with permission from (Abshirini et al. 2021); copyright 2021 John Wiley and sons.

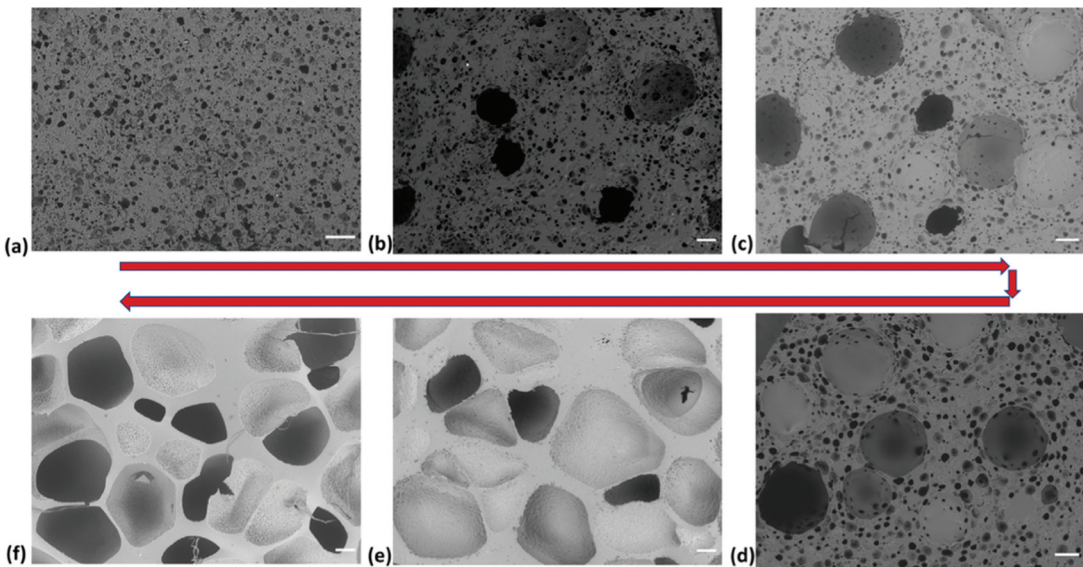


Figure 11. SEM images showing the porous microstructure in samples with (a) THF/solvent = 0:10, (b) THF/solvent = 2:10, (c) THF/solvent = 4:10, (d) THF/solvent = 6:10, (e) THF/solvent = 8:10, and (f) THF/solvent = 10:10 (scale bar is 200 μm in all images). (g) variation of the relative area fraction of large pores, ρ_L , with increasing THF/solvent ratio. (h) porosity of the samples with different microstructures fabricated from various solvent formulations. (i, j) stress – strain curve and the initial region for the porous samples with different microstructures and $\rho_L = 0\%$ (Thf/solvent = 0:0), $\rho_L = 30\%$ (Thf/solvent = 3:10), $\rho_L = 54\%$ (Thf/solvent ratio = 5:10), $\rho_L = 86\%$ (Thf/solvent ratio = 8:10), and $\rho_L = 100\%$ (Thf/solvent ratio = 10:10). (k) mechanical behavior of solid PDMS (Abshirini et al. 2021). Reprinted with permission from (Abshirini et al. 2021); copyright 2021 Elsevier.

experiments (Zhu, Handschuh-Wang, and Zhou 2017). However, it has the advantage of being able to be scaled up because controlling the pore size is possible and the fabrication process is simpler than the template method (Abshirini et al. 2020, 2021).

3. Applications of PDMS sponge

3.1. Sensors

Sensors are required for most electronic devices that are used in everyday life, such as smartphones, automobiles, and drones. The most important characteristics required by a sensor are high sensitivity, which enables it to react sensitively to external stimuli (Zhang et al. 2021), and stability, which helps it withstand deformation due to multiple presses. Because of its porous structure, compared to general bulk materials, PDMS sponge has a large surface area (Tan and Zheng 2022), high flexibility (Pan et al. 2020), and high compressibility (Pan et al. 2021; Tan and Zheng 2022). In addition, fillers are additionally used to enhance the aforementioned characteristics required for sensors (Li et al. 2022; Cao et al. 2019; Lv et al. 2022; Li et al. 2021, Li; Li et al. 2020, 2020; Zhao et al. 2019). This chapter summarizes the application of porous PDMS to sensors prepared by adding fillers such as Ag nanowires (AgNWs), graphene, and CNTs to PDMS.

3.1.1. AgNps based sensors

Paghi et al (Paghi et al. 2022) produced AgNP-coated PDMS sponge using the sacrificial template method. They measured the mechanical properties of the created AgNPs. Figure 14(a) shows cyclic stress – strain graph. It was measured under uniaxial loading/unloading cycles at a strain rate of 0.5 mm min^{-1} . The shape of the graph had a nonlinear form with hysteresis, and even under several cycles, both the common porous PDMS and AgNP-PDMS recovered to their original state without

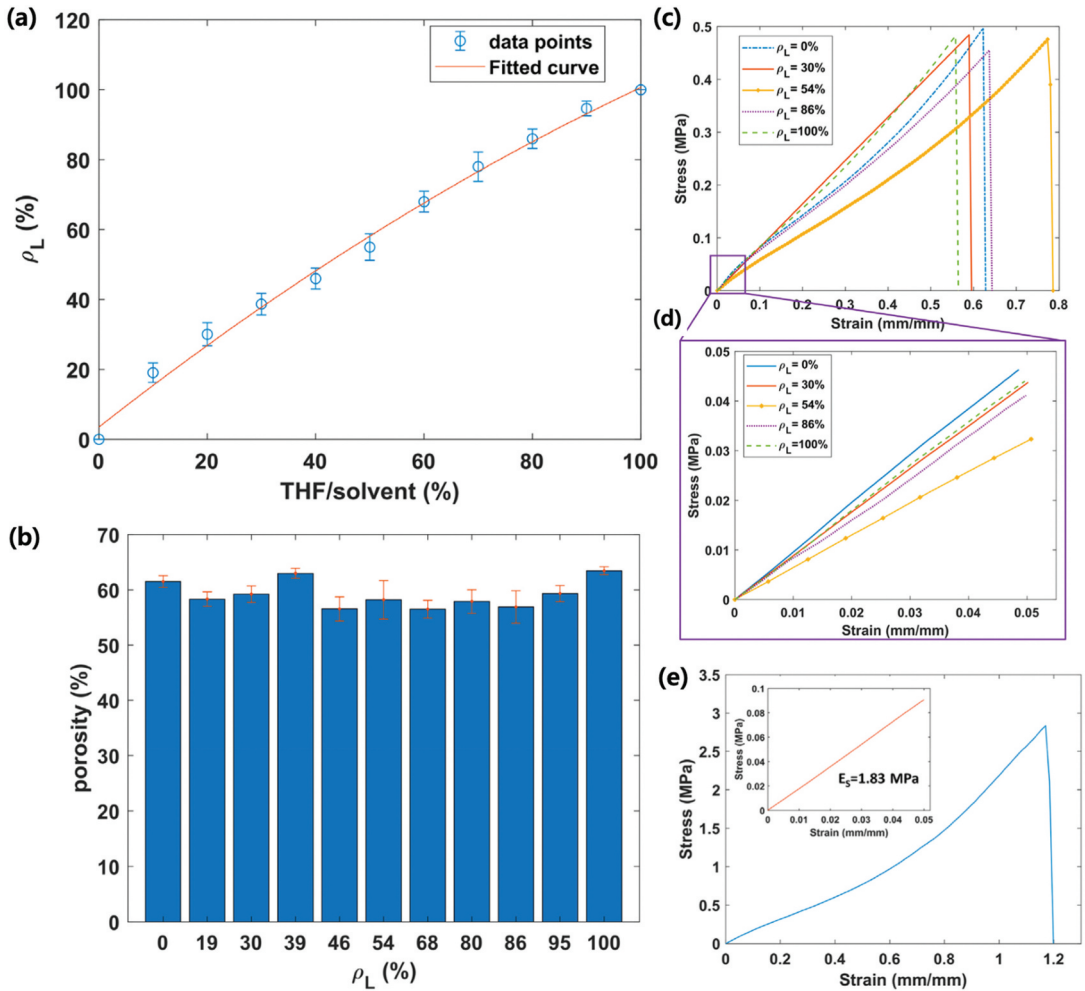


Figure 12. (a) variation of the relative area fraction of large pores, ρ_L , with increasing THF/solvent ratio. (b) porosity of the samples with different microstructures fabricated from various solvent formulations. (c, d) stress – strain curve and the initial region for the porous samples with different microstructures and $\rho_L = 0\%$ (Thf/solvent = 0:0), $\rho_L = 30\%$ (Thf/solvent = 3:10), $\rho_L = 54\%$ (Thf/solvent ratio = 5:10), $\rho_L = 86\%$ (Thf/solvent ratio = 8:10), and $\rho_L = 100\%$ (Thf/solvent ratio = 10:10). (e) mechanical behavior of solid PDMS (Abshirini et al. 2021). Reprinted with permission from (Abshirini et al. 2021); copyright 2021 Elsevier.

plastic deformation. There was a slight difference in stress values depending on the amount of AgNP; however, the curve shape was almost the same. Figure 14(b,c) shows the elastic modulus at strain < 10% and elastic modulus at strain < 55%, respectively. Under low strain, the general porous PDMS showed a modulus of ~ 70 kPa, and as the content of AgNP increased, it decreased to ~ 35 kPa and then tended to increase slightly at 16.6 mg. Under a high strain of 55% or more, the value was ~ 600 – 800 kPa regardless of the amount of AgNP.

Next, the characteristics of electrical properties were measured. AgNP-PDMS was inserted between two copper electrodes, and the $I - V$ curve was measured. The strain was measured by changing in the range of 0%–60%, and the shape of the $I - V$ curve was drawn linearly. This indicates the presence of a resistance path in which AgNPs are created by physical and electrical contact of NPs on the PDMS surface. By using Ohm's law in the $I - V$ curve, the resistance value according to strain is shown in Figure 14(d). When the strain value was 0, the higher the quantity of AgNPs, the lower was the resistance, and the resistance change according to the variation of the strain also decreased. This

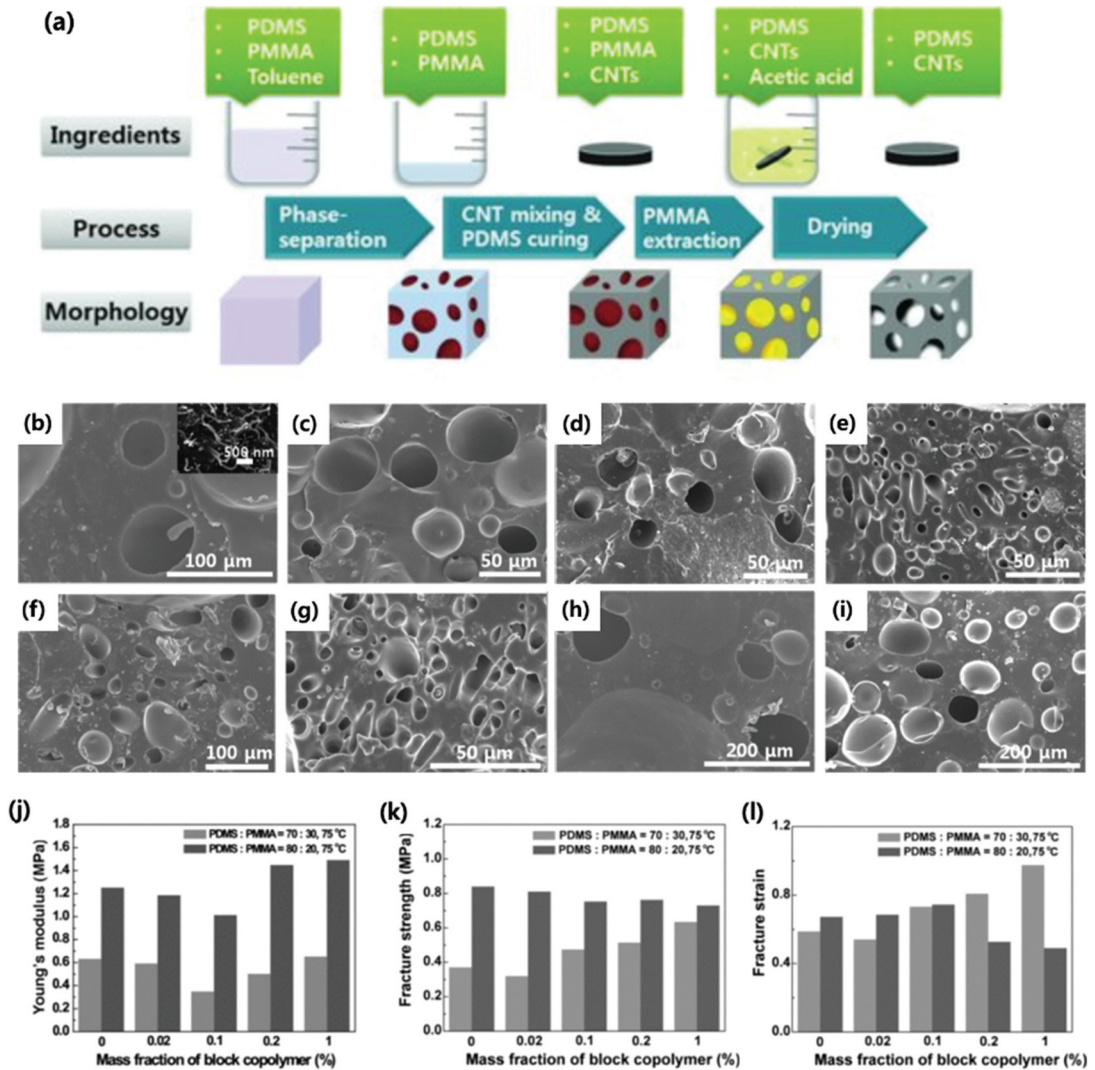


Figure 13. (a) the procedure to fabricate the porous PDMS-CNT nanocomposites. (b) SEM images of the porous morphologies of the samples prepared with different fractions of PMMA and the block copolymer in the initial mixture. The weight fraction of the embedded CNTs and the solvent drying temperature were fixed at 5% and 75°C, respectively. The weight fractions of the PMMA were (b – e) 20% and (f – i) 30%. The fractions of the PDMS – b-PMMA block copolymers were (b,f) 0.02, (c,g) 0.1, (d,h) 0.2%, and (e,i) 1%. The inset in (b) shows CNTs loaded in the nanocomposite. Statistical measurement data of (j) Young's modulus, (k) fracture strength, (l) fracture strain (Lee et al. 2012). Reprinted with permission from (Lee et al. 2012); copyright 2012 John Wiley and sons.

means that as the AgNP content increases, conductive paths increase, and as the strain level increases, additional conductive paths occur because of the porous structure. Finally, the most important factors in the sensor, gauge factor and sensitivity, were measured Figure 14(f,g). The gauge factor measured at a value where the strain level is less than 7.5% is called GF1, and the gauge factor measured when the strain level is more than 7.5% is called GF2. GF1 was 12.5, the highest value at 17.2 mg, and decreased as the mass of AgNP increased. Regarding GF2, there was a slight increase in the gauge factor as the AgNP content increased. The sensitivity showed a similar trend. S1, which denotes the sensitivity at the stress level of 5 kPa, showed the highest value of 0.41 kpa⁻¹ when AgNP was 17.2 mg, and the value decreased as the AgNP content increased. Furthermore, S2, which represents the sensitivity when the stress level is 5 kPa or more, showed a value between 0.001 and 0.003 kpa⁻¹ regardless of the AgNP

Table 1. Summary of mechanical properties, advantages and disadvantages of each methods.

| Method | Pore size | Stress | Strain (%) | Young's modulus | Advantage | Disadvantage | Remarks | Ref. |
|------------------------|---------------------------|--------------------------|------------------|------------------|---|--|-----------------------------------|-------------------------|
| 3D printing | - | | 85 | 2.44 MPa | Can make complex structures elaborately | Expensiveness of equipment | | (Woo et al. 2021) |
| Chemical foaming | 400 μm | 0.13 MPa | 64 | | Inexpensive and facile method | Hard to control pore size | Using NH_4HCO_3 , | (Long et al. 2018) |
| | 500 μm or more | ~ 4.5 kPa | 60 | | | | | |
| Sacrificial templating | GO/PDMS | ~ 11 kPa | 60 | | | | 0.1 wt% GO | |
| | GONR/PDMS | ~ 9.1 kPa | 60 | | | | 0.1 wt% GONR | |
| | CaCl_2 | 110 ± 20 kPa | 43 ± 6 | 220 ± 40 KPa | Not requiring expensive equipment, taking less time | Limited pore size by template material | Deliquescence method | (Keller et al. 2022) |
| | NaCl | 220 ± 50 kPa | 67 ± 8 | 250 ± 30 KPa | | | Water Immersion method | |
| | LiCl | $210 \pm 50 \mu\text{m}$ | 310 ± 60 kPa | 75 ± 8 | | | Deliquescence method | |
| Phase separation | Brown sugar | 80 ± 20 kPa | 41 ± 4 | 160 ± 50 KPa | | | Water Immersion method | |
| | White sugar | 140 ± 30 kPa | 50 ± 6 | 200 ± 40 KPa | | | Water Immersion method | |
| Phase separation | $\alpha = 1, 40\%$ PDMS | 0.23 MPa | 51 | 0.49 MPa | Easy to control pore size | Organic solvents are used in experiments | | (Abshirini et al. 2021) |
| | $\alpha = 8, 40\%$ PDMS | 0.9 MPa | 91 | 1.05 MPa | | | | |

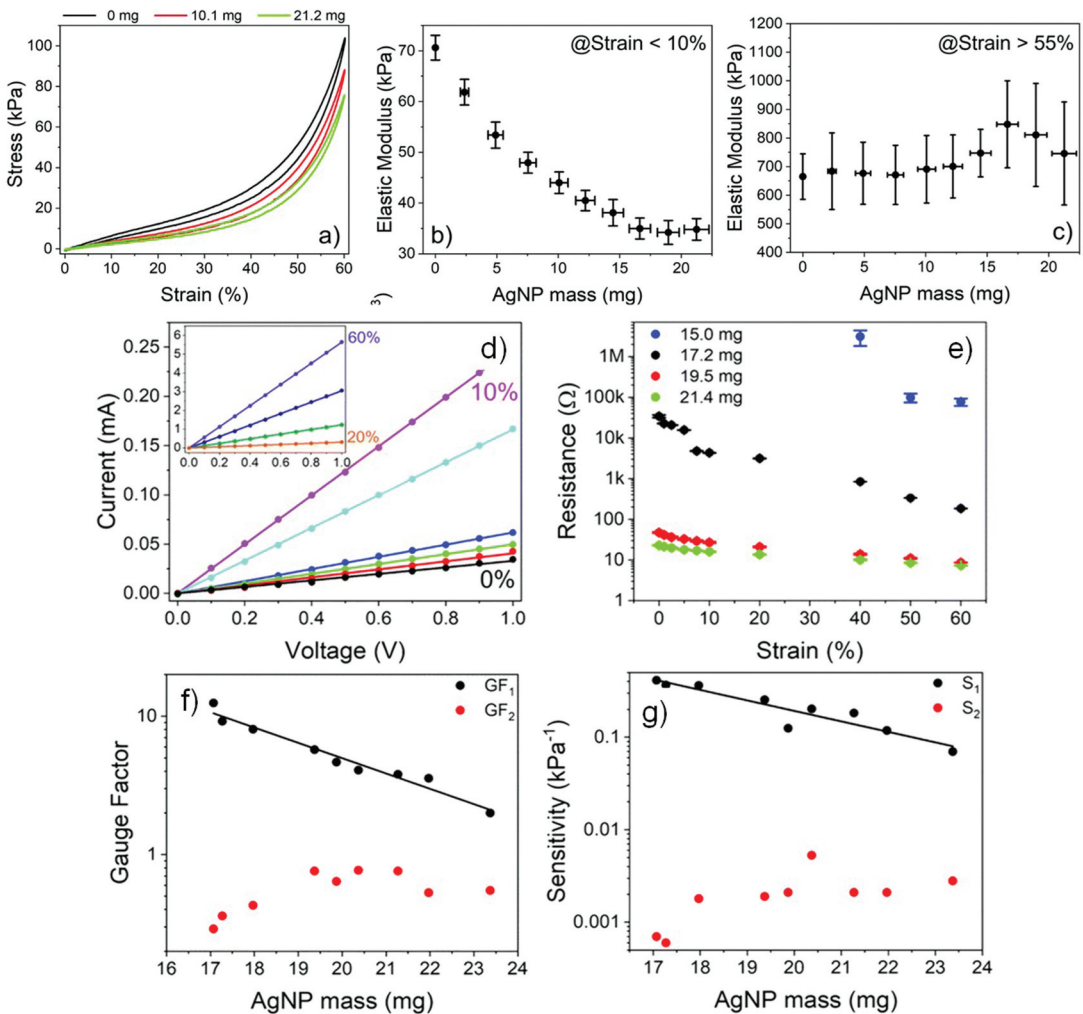


Figure 14. Mechanical characterization of PDMS foams decorated with AgNP networks. (a) stress – strain curves of PDMS foams with different AgNP masses. Data are measured under uniaxial loading/unloading cycles at a strain rate of 0.5 mm min⁻¹. (b) elastic modulus at strain level < 10%, (c) elastic modulus at strain level > 55%. (d) Current – voltage curves of a PDMS foam decorated with 17.2 mg of AgNPs measured in the range 0–1 V at different strain levels from 0 to 10%; the inset shows the current – voltage curves at strain levels ranging from 20 to 60%. (e) resistance – strain curves of PDMS foams decorated with different AgNP masses. (f) gauge factors of PDMS foams decorated with different AgNP masses, retrieved from the best fitting of normalized resistance variation – strain curves (dots). (g) sensitivity to stress of PDMS foams decorated with different AgNP masses, retrieved from the best fitting of normalized resistance variation – stress curves (dots) (Paghi et al. 2022). Reprinted with permission from (Paghi et al. 2022); copyright 2022 royal society of chemistry.

content. The increase in additional conductive paths caused by the porous structure means that the porous structure improves the performance of electronics, and the improvement of factors such as resistance and sensitivity according to the amount of AgNPs shows the importance of the fillers in the porous PDMS.

3.1.2. Ag nanowires (AgNws) based sensors

Tan et al (Tan and Zheng 2022). prepared a novel porous PDMS – AgNws – PDMS (PAP)-sponge-based capacitive pressure sensor. In the preparation of porous PDMS, the template technique and sugar were used. Then, an ethanol dispersion of AgNws was dropped on the dried sponge and it was pressed until

AgNWs were evenly dispersion. Finally, to obtain the PAP sponge, the AgNWs–PDMS sponge was immersed in PDMS solution to coat a thin PDMS film. To obtain the PAP sponge that exhibited the highest performance, the PAP sponge was created with different ratios of sucrose and white sugar: 0%, 33%, 50%, 67%, and 100%. The sensitivity was measured by applying a copper electrode above and below the PAP sponge at a pressure of 4 kPa. The ratio of sucrose to white sugar is expressed in m/M, where m is soft white sugar and M is the total mass of the sugar template. Sensitivity S can be defined as follows:

$$S = \frac{\frac{(C-C_0)}{C_0}}{\Delta P}, \quad (6)$$

where C is the capacitance under pressure, C_0 is the initial capacitance, and ΔP is the applied pressure. The results calculated according to this equation are presented in Figure 15(b). When a pressure of 4 kPa was applied, the sensitivity of the pure sucrose template was 0.1125 kPa^{-1} , which is approximately six times higher than that of a pure, soft white-sugar template. Thus, a 100% sucrose template is most suitable for a capacitive pressure sensor based on a PAP sponge. Tan et al. measured the sensitivity by changing the amount of AgNWs with a 100% sucrose template. Experiments were conducted for four cases: 50 (P-1), 100 (P-2), 150 (P-3), and 200 (P-4) mg of AgNWs; the results are presented in Figure 15 (c,d). The highest sensitivity was obtained for P-3 (at 62 kPa^{-1}), which showed a significantly higher value compared to many other capacitive pressure sensors.

Yang et al (Yang et al. 2021) produced porous AgNWs-PDMS/PVDF/PDMS by mixing poly (vinylidene fluoride) (PVDF) with PDMS. As the content of AgNWs increased from 40% to 57%, the sensitivity improved, and when the strain was 5% and 10%, the gauge factor was 212 and 653, respectively. These values are very high compared to those of other reported sensors, and it can be seen that the AgNW filler has a significant impact on sensor performance.

3.1.3. Carbon nanofiber-based sensors

Carbon nanofiber (CNF) is a promising material for flexible sensors owing to its high mechanical properties and stability (Qiang et al. 2019). Dai et al (Dai et al. 2021) prepared CNF/PDMS composites to produce a pressure sensor with excellent mechanical strength and high sensitivity. First, CNFs were added to xylene for dispersion, and then PDMS prepolymer was added to CNFs/xylene suspension. The suspension of CNFs and PDMS in xylene was stirred for 30 min at a speed of 3000 rpm/min. Then, Ni foam was dipped into CNFs/PDMS(CP)/xylene coating suspension. The CP/xylene-coated Ni foam was dried to remove xylene and immersed in HCl solution to remove the Ni skeleton to produce porous CNF-PDMS (CPF) Figure 16(a). Three samples with different pore structures were prepared while adjusting the weight ratio of xylene to PDMS (WR) and spin-coating time (t). (1T-Pore CPF (WR = 0:1; $t = 0$), 2T-Pore CPF (WR = 3:1; $t = 50 \text{ s}$), 3T-Pore CPF (WR = 5:1; $t = 60 \text{ s}$) Figure 16(b).

For the three samples, Dai et al. first measured the mechanical properties. As expected, there was a difference in the porous structure, thereby resulting in a difference in mechanical properties Figure 17(a-c). For 3T-pore CPF, a value of $\sim 12 \text{ kPa}$ was found at 80% strain, which was smaller than those of 2T-pore CPF and 1T-pore CPF. In the case of 2T-pore CPF and 3T-pore CPF, two distinct regions were found. When the strain was lower than 60%, elastic and plateau regions were found where the stress value did not change significantly even when the strain changed. This is because in the case of 2T-Pore CPF and 3T-Pore CPF, there is sufficient space for deformation to occur owing to a large number of pores. In the case of 60% strain or higher, a large pore is severely deformed, causing a reduction, which increases stress rapidly as the strain increases. In Figure 17(d), the durability of 3T-pore CPFs can be confirmed. One hundred cyclic compression tests were performed at 60% strain, with almost no change in stress. This shows the mechanical stability and flexibility of the 3T-pore CPFs.

Next, Dai et al. measured sensor properties Figure 17(e). They fabricated a sensor by inserting CPFs between two electrodes The S value of 3T-pore CPF was measured at 0.60 kPa^{-1} , which was a much

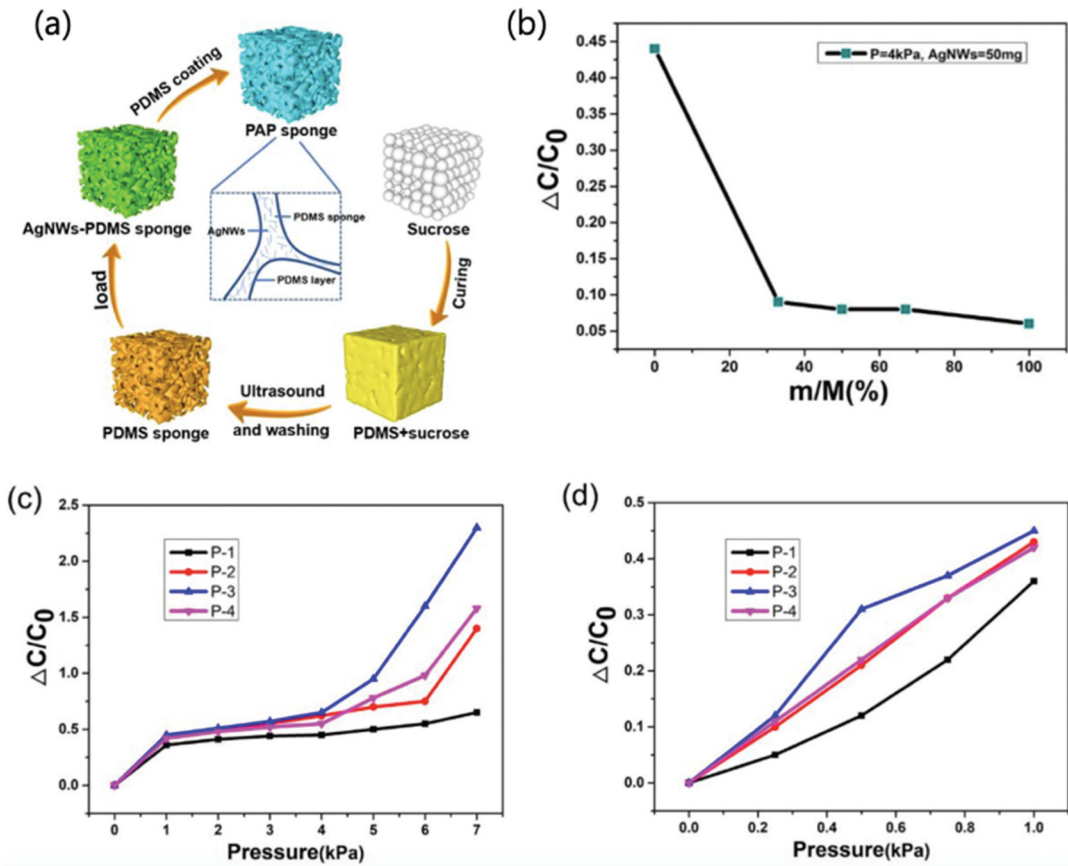


Figure 15. (a) schematic illustration of the fabrication processes of PAP sponge. (b) change curve of the capacitance change rate of PAP sponge by soft white sugar content in the template. (c, d) sensitivity curves of the capacitive pressure sensor with different loading amounts of AgNWs under applied pressure (Tan and Zheng 2022). Reprinted with permission from (Tan and Zheng 2022); copyright 2022 MDPI.

higher value than that of 1T-pore CPF (0.00007 kPa^{-1}) and 2T-pore CPF (0.08 kPa^{-1}). As the pressure increased, the sensitivity of 3T-pore CPFs was 0.08 kPa^{-1} in the 1–6 kPa section and 0.01 kPa^{-1} in the 6–20 kPa section, as in the case of 2T-pore CPFs. The sensitivity value of 3T-pore CPF, $\sim 0.60 \text{ kPa}^{-1}$, is much higher than the sensitivity of composite materials based on PU (Li et al. 2019; Wu et al. 2016; Zhong et al. 2019).

The above results can be attributed to the multilevel pore structure. In addition, CPF, which shows better sensitivity than that obtained using other polymers and fillers, clearly shows the utility of CNF.

3.1.4. CNT-based sensors

CNTs are most commonly used as a filler (Turco et al. 2023; Zhao et al. 2022) because of their excellent mechanical strength (Peng et al. 2014) and high electrical conductivity (Peng et al. 2014) similar to copper. Song et al (Song et al. 2017) produced a CNT – PDMS sponge electrode to create a material that could exhibit high performance for use in a piezoresistive sensor (PRS).

Figure 18(a) schematically shows the general CNT – PDMS sponge process. A PDMS sponge is produced by dropping PDMS on the prepared sugar cube. The PDMS is tightly filled in the empty space of the sugar tube by the capillary action. To control the concentration of CNTs, the coating is performed while modulating the drop-drying cycle to obtain a CNT – PDMS sponge with desired characteristics. The morphology of the PDMS sponge and CNT – PDMS sponge was

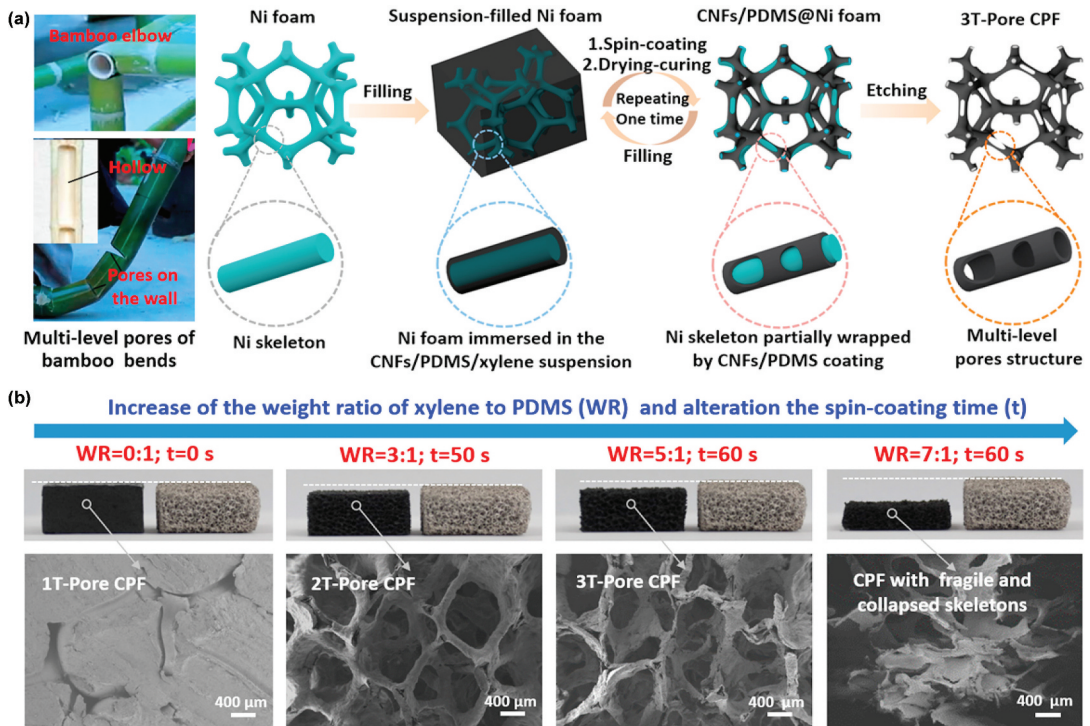


Figure 16. (a) schematic for fabrication process of the 3T-pore CPF via simply adjusting the coating viscosity (the weight ratio of xylene to PDMS) and applying the spin-coating process. (b) the photos and SEM morphologies of prepared CPF samples with different pore structures under different processing conditions (Dai et al. 2021). Reprinted with permission from (Dai et al. 2021); copyright 2021 Elsevier.

confirmed by SEM. From Figure 18(b), it can be confirmed that an open network of pores is well formed in the place where the sugar cube is located; thus, it could appropriately act as a porous material. Figure 18(c) shows the SEM image of the completed CNT – PDMS, revealing that the surface of the scaffold is rugged.

Figure 19(b) shows a stress – strain graph measured under different compressive strains. For $\epsilon < 10\%$, the stress value does not change significantly even if the sponge is deformed. This can be described as an elastomeric region. In the case of $10\% < \epsilon < 45\%$, the graph is relatively a plateau and the scaffold is buckled and collapsed. If ϵ exceeds 45%, the PDMS scaffold is crushed and acts like bulk material, indicating exceptional mechanical performance. Figure 19(c) presents the stress – strain graph of the CNT – PDMS sponge and PDMS sponge under 60% strain. The graph has almost the same shape, but it can be seen that the CNT – PDMS sponge is more resistant to compression, indicating that the mechanical properties have been improved by the CNT filler. Finally, Figure 19(d) shows the stability of the CNT – PDMS sponge. There was almost no change in resistance under 200 compressing – releasing cycles

To measure the PRS performance of the CNT – PDMS sponge, as shown in Figure 20(a), a CNT – PDMS sponge was inserted between the two electrodes of PET/ITO. The resistance response was measured through a voltage signal generated by a force applied to the top surface. The resistance response value was calculated as $\Delta R/R_0 = (R_0 - R_x)/R_0$, where R_0 and R_x denote the resistance without and with compressive stress, respectively. Figure 20(b) shows the current – voltage (I – V) characteristics of PRS under various compressive stresses. From the graph, it can be verified that linear I – V characteristics are manifested even under various compressive stresses. Figure 20(c) shows the plot of $\Delta R/R_0$ versus applied compressive stress. The sensitivity (S) value,

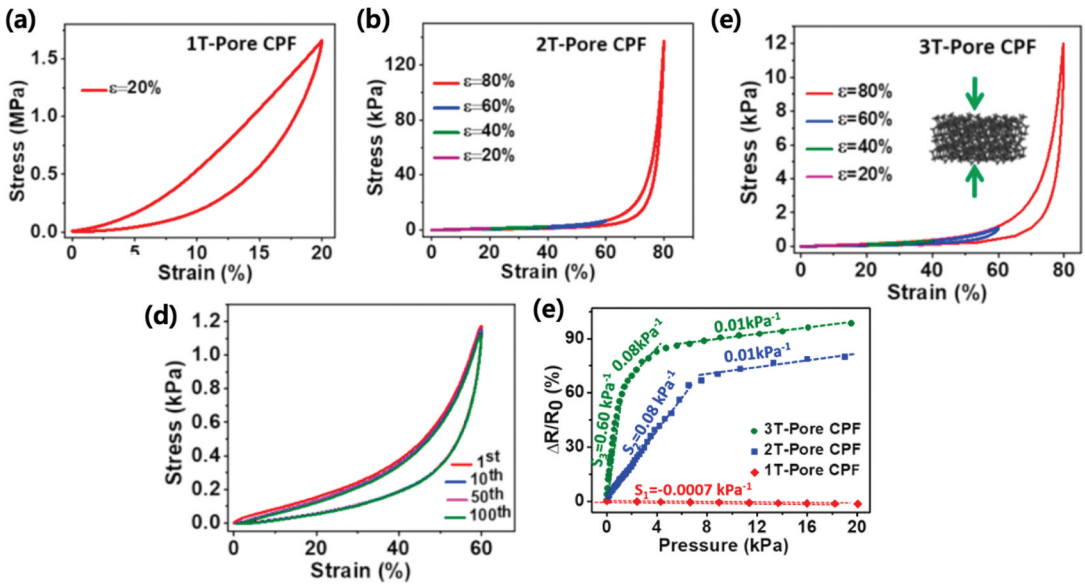


Figure 17. Compressive stress-strain curves of CPFs with different pore structures: (a) 1T-pore CPF at the strain of 20%. (b, c) 2T-pore CPF and 3T-pore CPF at the maximum strains of 20%, 40%, 60% and 80%, respectively. (d) cyclic compressive stress-strain curves of the 3T-pore CPF at 60% strain for 100 cycles. (e) relative resistance variations of the sensors based on three different pore structures (Dai et al. 2021). Reprinted with permission from (Dai et al. 2021); copyright 2021 Elsevier.

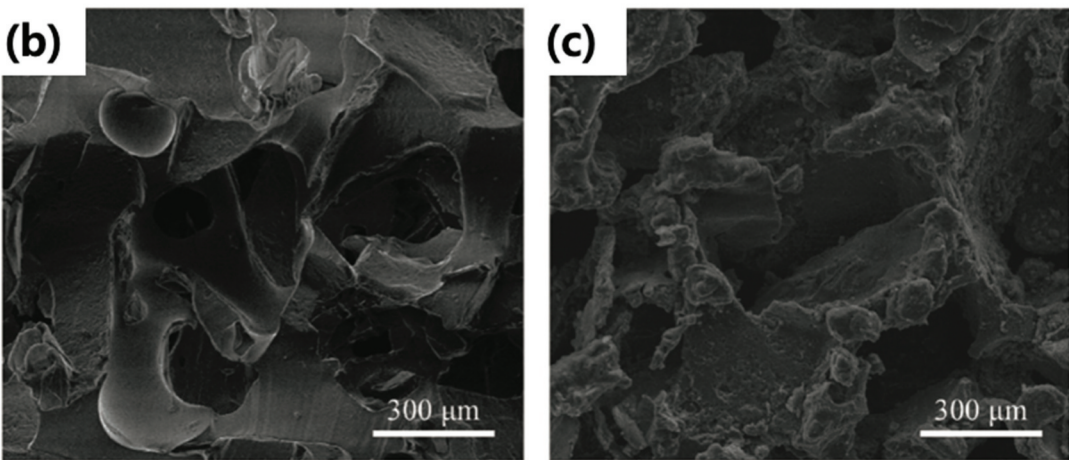
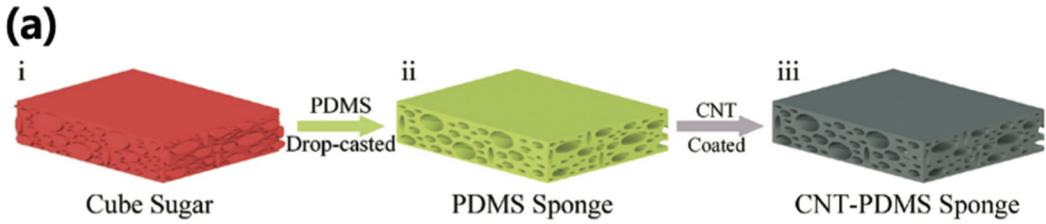


Figure 18. (a) fabrication process of the CNT – PDMS sponge. SEM images of the b) PDMS sponge and c) CNT – PDMS sponge (Song et al. 2017). Reprinted with permission from (Song et al. 2017); copyright 2017 John Wiley and sons.

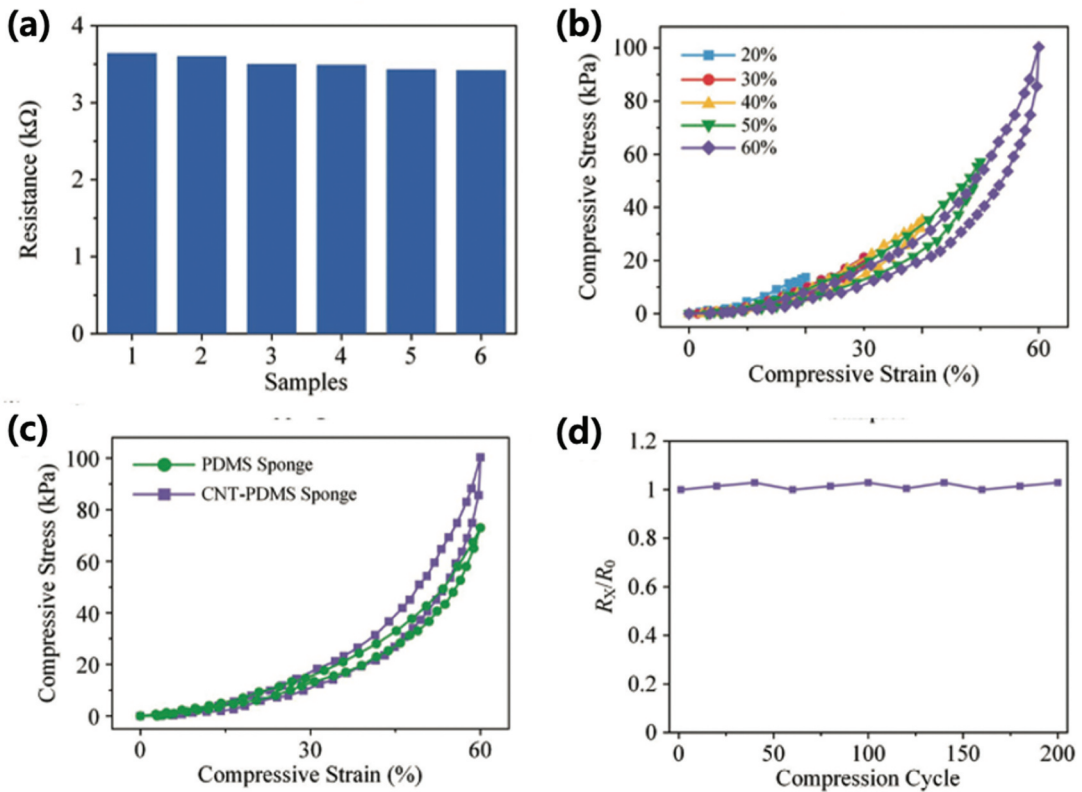


Figure 19. (a) resistance histogram of six CNT – PDMS sponges after 10 drops. (b) compressive stress – strain curves of CNT – PDMS sponge at different strains (20%–60%). (c) compressive stress – strain curves with a maximum strain of 60% for the PDMS sponge and CNT – PDMS sponge. (d) stability of the electrical resistance of the CNT – PDMS sponge in the first 200 compressing – releasing cycles (Song et al. 2017). Reprinted with permission from (Song et al. 2017); copyright 2017 John Wiley and sons.

considered the most important in a sensor, is obtained from the slope of the graph and can be defined as follows:

$$S = \delta(\Delta R/R_0)/\delta P, \quad (7)$$

In Equation 10, P denotes the compressive stress. The sensitivity in the first 0–15-kPa section represents a value of 0.03 kPa^{-1} . After the conductive scaffold of the CNT – PDMS sponge is fully contacted, the 25–50 kPa section shows a sensitivity reduction by 0.008 kPa^{-1} . In addition, in Figure 20(d), which shows the resistance response according to the repeated compressing – releasing cycles, low stress (26 Pa) is detected. The CNT – PDMS sponge is a versatile material that can be used in any type of sensor, which is confirmed by its good sensitivity and very low compressive stress (26 Pa).

3.1.5. Graphene-based sensors

Several studies are being conducted to improve the mechanical stability and electric conductivity of polymers. In particular, a method of coating or synthesizing nanomaterials into porous sponges is attracting researchers' attention (He et al. 2021; Pan et al. 2021). Graphene is a carbon-based material and has a layered structure. Because of its excellent mechanical strength owing to sigma bonding (Bekyarova et al. 2013), it is widely used to improve the mechanical properties of PDMS sponge (Zhao et al. 2022).

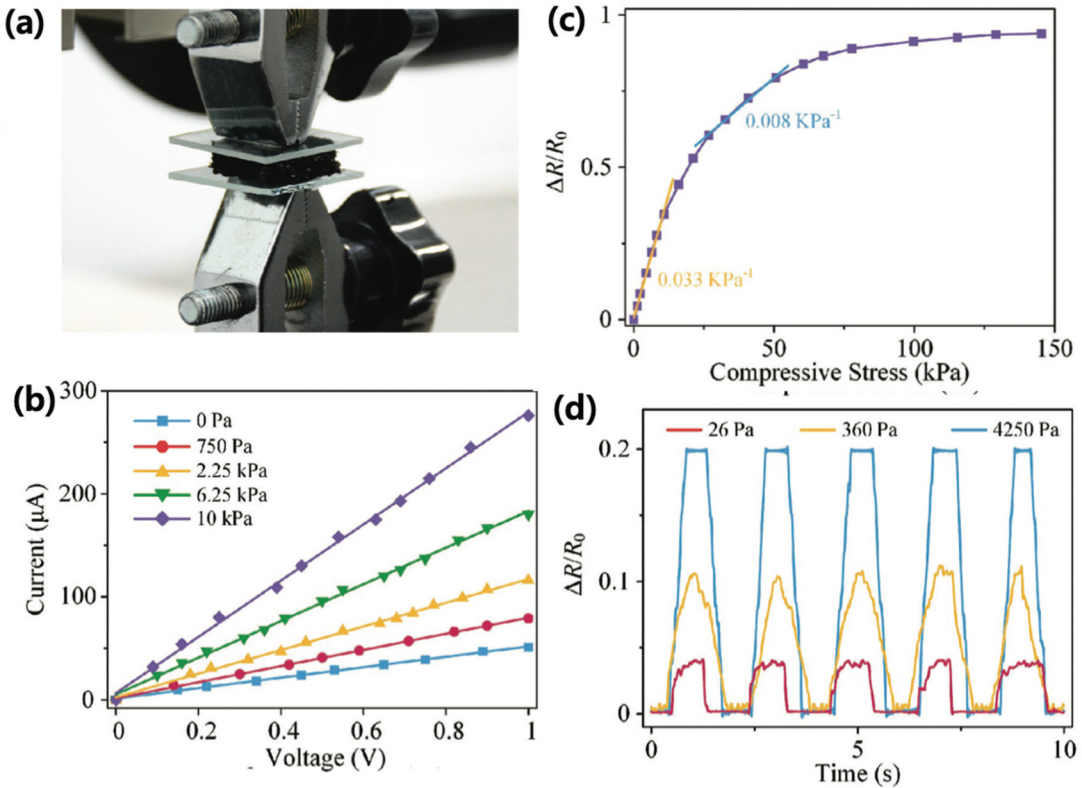


Figure 20. (a) Piezoresistance measurements of the PRS with the push – pull gauge. (b) Current – voltage ($I - V$) curves of PRS under different compressive stresses. (c) stress-response curves for PRS, the sensitivity of which reaches 0.03 kPa^{-1} . (d) resistance responses of repeated compressing – releasing cycles with different stresses (Song et al. 2017). Reprinted with permission from (Song et al. 2017); copyright 2017 John Wiley and sons.

Jung et al (Jung et al. 2019) prepared conductive, flexible, and stretchable graphene-coated PDMS through the sugar-templating process and the dip-coating method. They measured tensile stress – strain curves under different maximum strain ranges; the mechanical properties of bare PDMS sponge and graphene-coated PDMS sponge were obtained under 20% strain and 1000 cycles Figure 21(a-c). The bare PDMS sponge required 72.9 kPa of stress for 77.7% strain, and the graphene-coated PDMS sponge required 80.9 kPa of stress for 68% strain. For the same amount of deformation, more force should be applied to the graphene-coated PDMS, indicating that its mechanical properties are superior to those of a bare PDMS sponge. In addition, the tensile stress – strain curve was measured under variable strain, revealing that the maximum stress also increased as the strain increased. Figure 21(c) shows a graph for the cycling test. Figure 21(c) reveals that the stability is excellent, considering that there is no significant change in the stress – strain curve shape even after 1000 cycles.

The characteristics of the graphene-coated PDMS sensor were measured under static loads. Figure 22(a) shows the relative resistance variation when stretching and releasing are performed under strains ranging from 0% to 40%. There was no significant change in resistance up to 10%, but it increased steeply in the 10%–30% range. In the case of stretching and releasing, the graphs are almost identical, which means that hysteresis rarely occurs owing to the reversible deformation characteristics of the pore. Figure 22(b) shows a graph drawn by measuring the value of voltage (V) versus current (I) under different strains. Ohm's law indicates resistance in the $V - I$ graph, which can be interpreted as the resistance changing significantly depending on the value of strain. Figure 22(c) shows a graph depicting the change

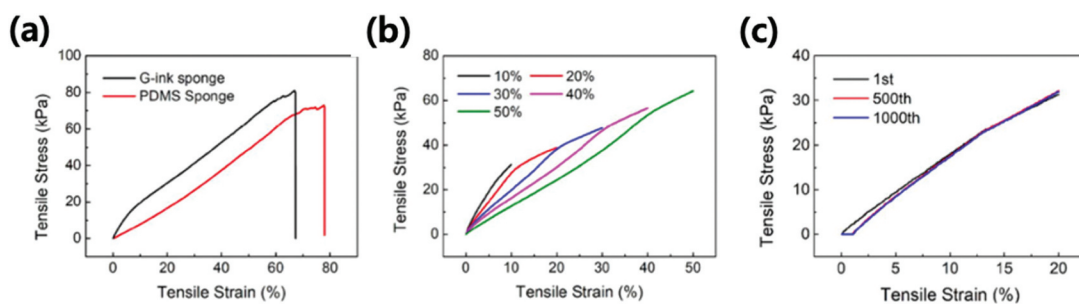


Figure 21. (a) measured tensile stress – strain curves of bare and graphene-coated PDMS sponges. (b) tensile stress – strain curves under different maximum strains (from 10% to 50%). (c) measured results for 1000 cycles under 20% strain (Jung et al. 2019). Reprinted with permission from (Jung et al. 2019); copyright 2019 Springer nature Switzerland AG. Part of Springer nature.

in relative resistance for 15 cycles over time under various maximum strains ($\Delta R/R_0 = \frac{R-R_0}{R_0}$, where R and R_0 denote resistance values with and without applied strain, respectively). Measurements were performed within a strain range of 5%–50%. In the case of 5% strain, the $\Delta R/R_0$ value differed from the value of the first and last cycles; however, in the case of 10% or more strain, the value did not change significantly even after several cycles. From this result, it can be seen that graphene-coated PDMS can provide stable performance even under various strains. The sensitivity (gauge factor, $\delta(\Delta R/R_0)/\varepsilon$, where ε denotes applied strain) was calculated under a strain ranging from 10% to 50% as follows: 3.63, 6.43, 8.82, 13.09, and 19.21. Thus, the sensitivity increased as the strain increased. A value of 19.21 under 50% strain indicates that the graphene-coated PDMS sponge can sufficiently detect human body motion and act as a sensor.

Zhao et al (Zhao et al. 2022). also produced porous CNTs/graphene PDMS by mixing CNT and graphene. The graphene nanosheet created a conductive graphene framework on the surface of the PDMS, and CNTs were uniquely dispersed over the graphene nanosheet. Graphene acts as a structure, and CNTs have a high aspect ratio, which simultaneously improves mechanical and electrical properties, leading to an improvement in sensor properties. Because of this synergistic effect, porous CNTs/graphene PDMS showed a high sensitivity value of 300.31 kPa^{-1} at 0–200 kPa.

In addition to 1D and 2D materials such as CNT, CNF, and graphene, 0D materials such as carbon black (CB) are also used for sensors. Pruvost et al (Pruvost et al. 2019) produced CB/PDMS capacitive sensors by dropping and distributing CB evenly on PDMS. CB/PDMS using CB materials that are easy to prepare and have high-capacity value have shown higher sensitivity and capacity performance than general porous PDMS. Table 2 presents the characteristics of the sensor according to the materials.

In this way, various fillers including organic and inorganic materials can be used to obtain the desired sensor properties. Mechanical, electrical, and sensor properties may be dramatically improved by not only using a single material but also mixing and using various materials and utilizing the synergistic effect. There are limitations in the number of substances present, but there are numerous cases of combining them. Therefore, studies on discovering new materials as well as developing new combinations of extant materials are essential.

3.2. Flexible electrode for supercapacitors

With the recent development of portable and wearable technologies, flexible energy-storage devices have attracted the attention of many researchers (Song et al. 2020). Supercapacitors (SCs), one of the energy-storage systems, have high power densities and long cycle life (Lee, Wee, and Hong 2015). In SCs, electrodes are one of the most important elements. The electrode used in flexible SCs should have

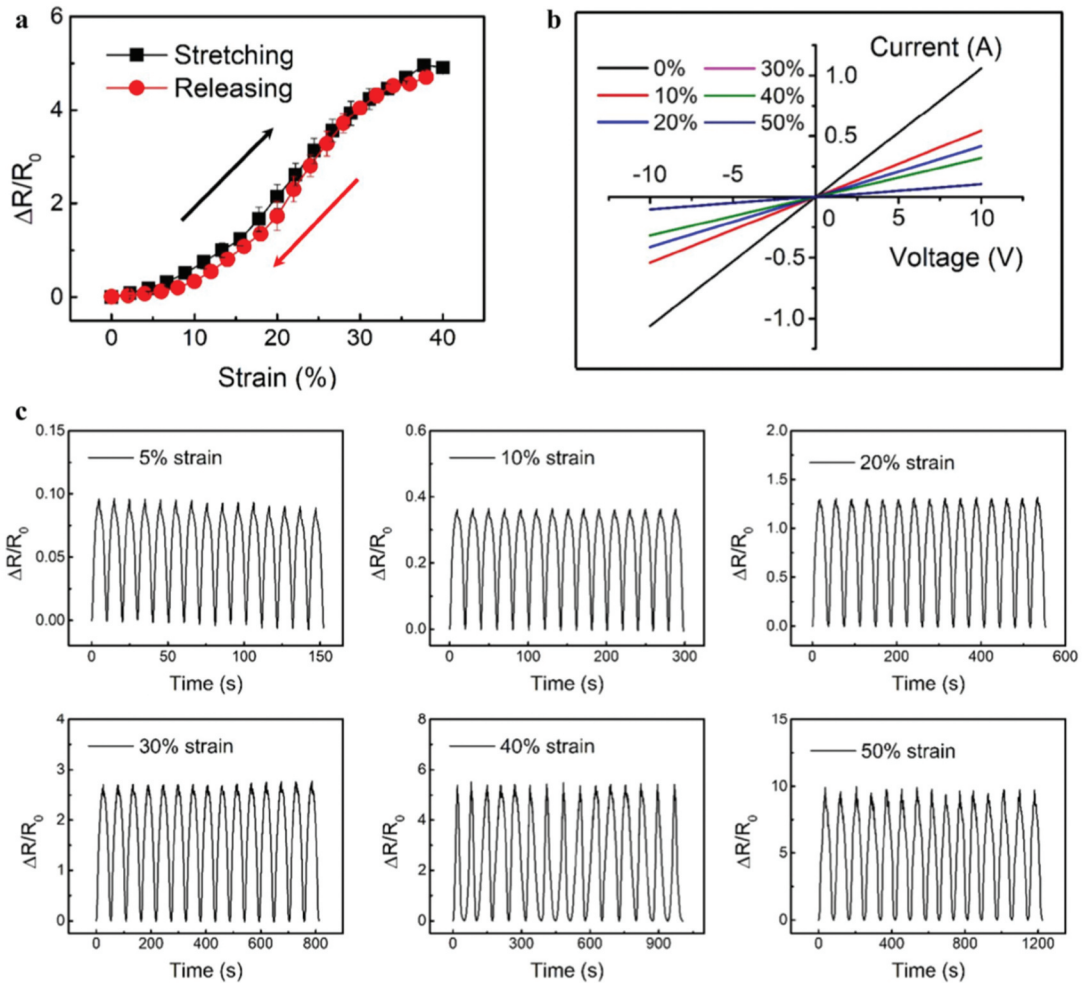


Figure 22. Measured sensing performance of the piezoresistive strain sensor based on the graphene-coated PDMS sponge. (a) relative resistance variation of the strain sensor under 40% strain with stretching/releasing. (b) voltage versus current characteristics of the sponge under different strains. (c) measured relative change over 15 cycles according to time with various maximum strains (Jung et al. 2019). Reprinted with permission from (Jung et al. 2019); copyright 2019 Springer nature Switzerland AG. Part of Springer nature.

high energy-storage performance and should not lose its electrical properties even after several deformations. The sponge structure of the PDMS sponge can be applied to flexible electrodes because it has high porosity and thus a large surface area and durability under pressure.

Pecenek et al (Peçenek et al. 2022). fabricated a NiO/MnO₂/CNT sponge by coating NiO/MnO₂/CNT composite on PDMS sponge fabricated with the sugar template method. The cyclic voltammetry (CV) curves of the prepared PDMS sponge were obtained at different scan rates between 0.2 and 0.55 V. Figure 23(a) reveals that the shape of the curve appears stable at various scan rates owing to the characteristic of high rate capability. Figure 23(b) shows the test graph before and after cycling at a scan rate of 100 mV/s. Both CV curves show clear redox peaks, and the shape is not much different. Figure 23(c) shows the CV curve for the pressed and released states. There is no significant difference between oxidation and reduction peaks, and the overall graph shape is similar. This means that compression does not significantly affect the performance of the sponge electrode. CV tests were also conducted under various bending angles to measure the flexibility of the sponge.

Table 2. Summary of pore size, sensitivity and gauge factor of each sensors depending on materials.

| Materials | method | Pore size | Pressure (kPa) | Sensitivity (kpa ⁻¹) | Gauge factor | remarks | reference |
|------------------|-------------------------------|------------------|----------------|----------------------------------|--------------|---|----------------------|
| Ag nanoparticles | Sacrificial templating method | 279 ± 50 μm | 5 | 0.41 | 12.5 | Strain level < 7.5% | (Paghi et al. 2022) |
| Ag nanowires | Sacrificial templating method | | More than 5 | 0.001 ~ 0.003 | ~1 | Strain level > 7.5% | (Tan and Zheng 2022) |
| CNF | Ni foam template | | 1-6 | 0.00007 | | Ag nanowire 150 mg WR = 0:1; t = 0 s | (Dai et al. 2021) |
| | 1T-pore CPF | | | 0.08 | | WR = 3:1; t = 50 s | |
| | 2T-pore CPF | | | 0.60 | | WR = 5:1; t = 60 s | |
| | 3T-pore CPF | | | 0.03 | | | (Song et al. 2017) |
| CNT | Sugar cube template | | 0-15 | 0.008 | | | |
| | | | 25-50 | | | | |
| | | | ~0.02 | 38.5 | 32 | PDMS:Hexane = 3:2 | (Turco et al. 2023) |
| | Sugar template | 626.2 ± 203.2 μm | ~0.02 | 47.8 | 32 | PDMS:Hexane = 1:1 | |
| | | 452.3 ± 145.9 μm | ~0.02 | 330 | 85 | PDMS:Hexane = 2:3 | |
| | | 440.7 ± 134.9 μm | ~0.02 | | | | |
| CNT/graphenes | Microwave irradiation | 400 μm | 0-50 | 300.31 | | | (Zhao et al. 2022) |
| | | | 50-200 | 52.51 | | | |

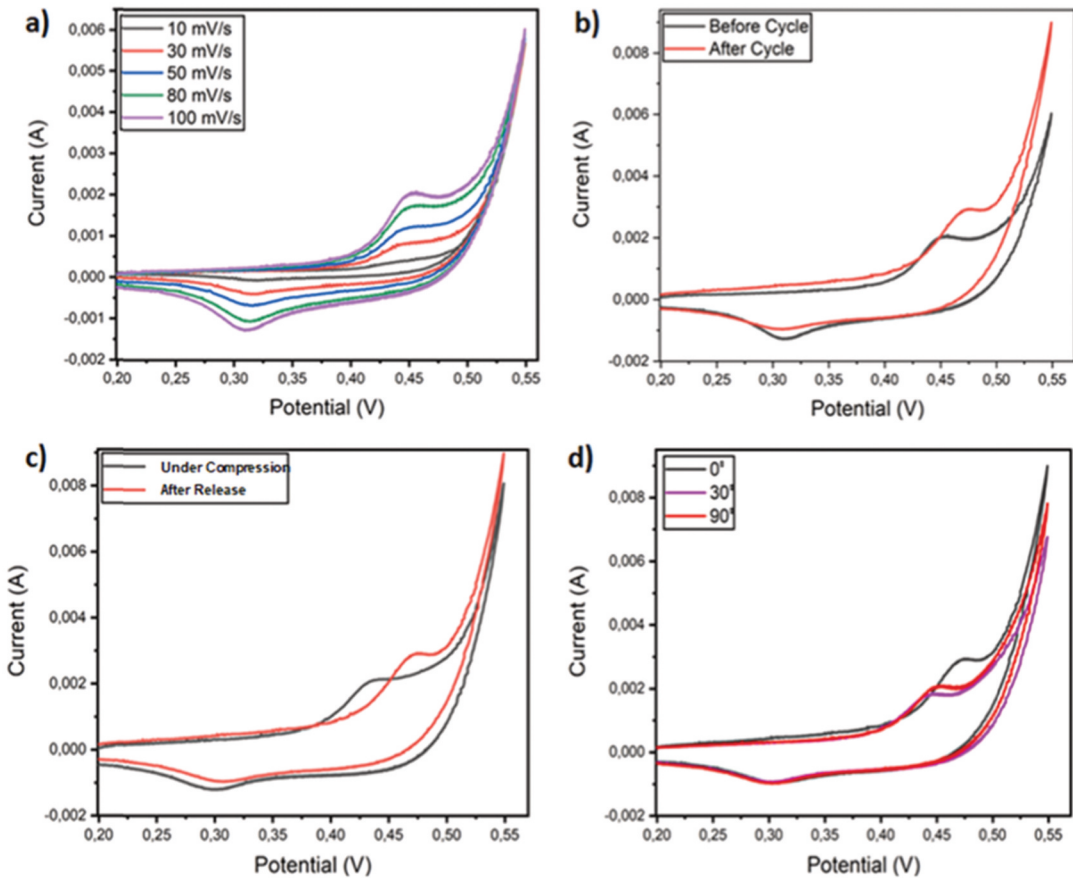


Figure 23. CV curves of NiO/MnO₂/CNT sponge electrode (a) at different scan rates. (b) before and after cycling. (c) under compression and without compression. (d) under bending at different angles (Peçenek et al. 2022). Reprinted with permission from (Peçenek et al. 2022); copyright 2022 Elsevier.

Figure 23(d) shows that there is little potential difference even when the bending angle is changed. Under 10,000 cycles, the capacity of the NiO/MnO₂/CNT sponge was 23 F/g at 0.1 A/g. This value is not high compared to the capacitance value when using general materials. However, the sponge fully recovered even after more than 10,000 compressive cycles, exhibiting a performance similar to the first time. This result is significant because such characteristics of the sponge are very important in wearable devices. This shows that a sponge-like electrode can be used for flexible and wearable devices.

In addition, materials containing graphene, such as chemically reduced graphene oxide and graphene oxide reduced in propylene carbonate, are also used as electrodes owing to the high surface area properties of graphene (Stoller et al. 2011). Huang et al. (Huang et al. 2021) created electrodes on flexible capacitive pressure sensors using Laser-Induced graphene. Because of the characteristics of the high surface area of graphene, electrodes with high capacity could be obtained.

3.3. Nanogenerators

With the recent development of wireless sensor networks and flexible and wearable technologies, the importance of stretchable and highly efficient power supplies is growing (Gao et al. 2021).

Accordingly, various studies on triboelectricity and electronic effect-based triboelectric nanogenerators (TENGs) are currently being conducted (Kim et al. 2021; Zhang et al. 2021). TENGs are a promising choice with applications in self-powered biosensor systems (Lu et al. 2022; Wang et al. 2022) and thin and wearable electronic devices (Wang et al. 2021) owing to their simple design and process, affordability, and light weight.

The materials generally used in TENGs include polymers and metals. Among them, PDMS is widely applied in TENG dielectric tribo-materials because of its advantages such as high electronegativity, flexibility, and biocompatibility. In particular, many studies have recently been conducted using a sponge-type PDMS with a porous structure to increase the performance of TENGs, such as an increase in the friction area and high surface charge densities (Tantraviwat et al. 2020).

Tantraviwat et al (Tantraviwat et al. 2020) produced a highly porous PDMS using silicon molds with a nanograss pattern. After thermally growing silicon dioxide on a wafer, the nanograss pattern was created through the dry-etching method. A PDMS mixture was put in the prepared silicon molds and spin coating was performed at 300 rpm for 60 s. Subsequently, a TENG was produced by laminating a PET/ITO film. The process conditions are shown in Figure 24(a-d).

To measure and compare the energy-harvesting performance, we created TENGs with three different PDMS surfaces: porous (S1), micropillar (S2), and flat (S3) patterns. The electrical properties of the TENG were evaluated by measuring the voltage and current outputs generated by the periodic application of external force.

No electric potential is generated when the two triboelectric layers are not in contact. However, the moment a force is applied and the PDMS comes in contact with aluminum, the PDMS pulls the electrons from aluminum because of the difference in electron affinity. Next, when the applied force is released, an electrical signal is generated as a current flows through an external circuit owing to the potential difference between the top and bottom electrodes. Then, when a force is applied again, the electrons flow again in the opposite direction to generate an electrical signal. According to this principle, an alternating current occurs when a periodic force is applied to the TENG.

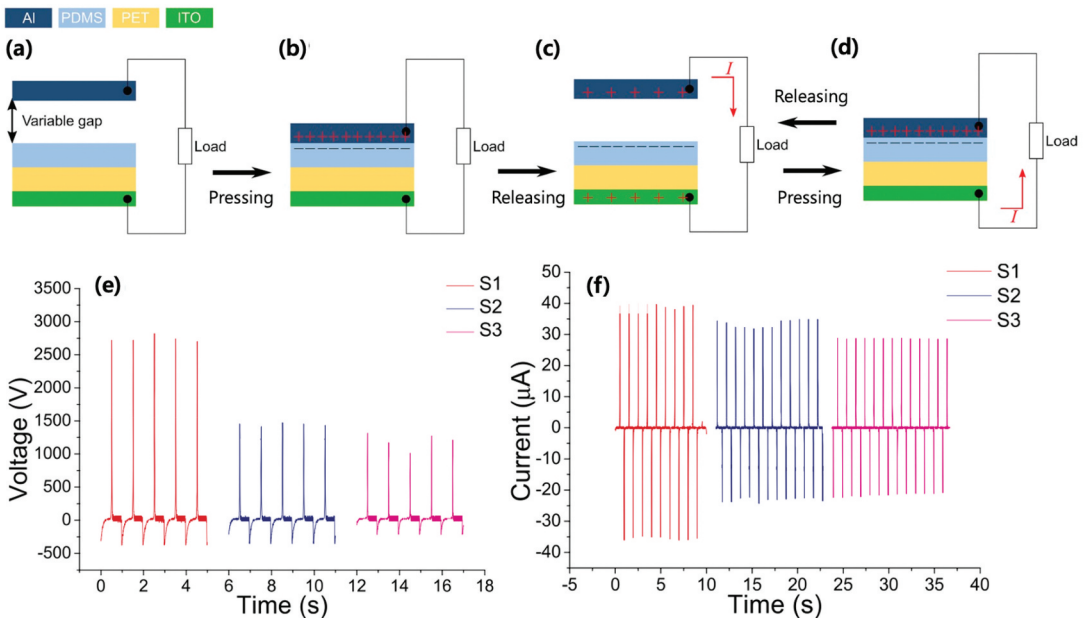


Figure 24. (a–d) illustration of the operating principle of patterned PDMS-based TENGs. An alternating current is generated under periodic contact and separation. (e, f) output performance of the TENGs with a gap of 1 mm and frequency of 1 Hz (Tantraviwat et al. 2020). Reprinted with permission from (Tantraviwat et al. 2020); copyright 2020 Elsevier.

Figure 24(e, f) shows a graph of the measured output voltages and currents at 1 Hz for three TENGs (S1, S2, and S3). S1 showed the highest value for both voltage and current. In the case of voltage, a peak of ~3200 V was observed, which was approximately twice as high as those of S2 and S3; the current did not show a significant difference, but it showed the highest value. Compared to general PDMS, porous PDMS has characteristics of high surface robustness and large contact electrification area. Because of these characteristics, additional charge is generated by electrostatic effects in the inner or surface pores, resulting in high electrical performance; therefore, porous PDMS is in the spotlight as a promising material that can improve the performance of TENGs.

3.4. Oil/Water separation

Ozkan et al (Ozkan et al. 2023) produced porous PDMS with superhydrophobicity, conductivity, and highly efficient oil/organic solvent – water separation properties using the sacrificial templating method. In addition, 1 H,1 H,2 H,2 H-perfluorooctyltriethoxysilane(FAS)-treated hydrophobic GR platelets and Cu microparticles were added to the PDMS network. The most important characteristic of oil/organic solvent – water separation is adsorption capacity. The admission capacity (M) may be expressed as follows.

$$M(\%) = \frac{m_1 - m_0}{m_0} \times 100\%, \quad (8)$$

where m_0 and m_1 are the weights of the foam before and after the adsorption test, respectively.

Ozkan et al. conducted an experiment by fixing m_{GR} , m_{Cu} to 10 wt% by the weight of PDMS and changing PDMS and NaCl using chloroform as an organic solvent. The adsorption capacity generally increased as the porosity increased. When $m_{PDMS} : m_{NaCl}$ was 1:14, it showed the highest porosity of 85.2%, and accordingly, the adsorption capacity also showed a value of more than 1600%, which was the largest value.

In addition, the experiment was conducted by changing the content of graphene in a condition where $m_{PDMS} : m_{NaCl} : m_{Cu} = 1:10:0.1$. As the graphene content increased to 0%–30%, the porosity decreased. Consequently, the adsorption capacity also decreased; when graphene was 0%, the adsorption capacity was ~1500%, and when it increased to 30%, the adsorption capacity decreased to ~1100%. Additionally, for various oils and organic solvents, $m_{PDMS}:m_{NaCl}$ was fixed at 1:10, and then the adsorption capacity was measured; it ranged from $221.3 \pm 16.9\%$ to $1249.5 \pm 33.8\%$ Figure 25(e). This means that the adsorption capacity can also be changed by the characteristics of the oil.

Further, Ozkan et al. calculated separation flux and efficiencies by mixing chloroform, dichloromethane, and hexane with water to measure the filtering capacity for oil/organic solvent – water separation. Separation efficiency (SE) and flux (J) are defined as follows:

$$SE(\%) = \frac{m_a}{m_b} \times 100\%, \quad (9)$$

$$J = \frac{V}{tA}. \quad (10)$$

As shown in Figure 26(a,b), all three solvents showed separation efficiencies > 99%. Thus, PDMS-GR-Cu can play an effective oil/water separation role without any performance degradation even after several cycles.

4. Summary and outlook

In this article, we first discussed the processing method for PDMS sponge and its different properties. There are various processing methods for PDMS sponges, such as 3D printing, gas foaming, sacrificial tempering, and phase separation. Porous PDMS prepared by each method showed superior mechanical properties compared to the bulk counterpart PDMS. For example, Woo et al (Woo et al. 2021).

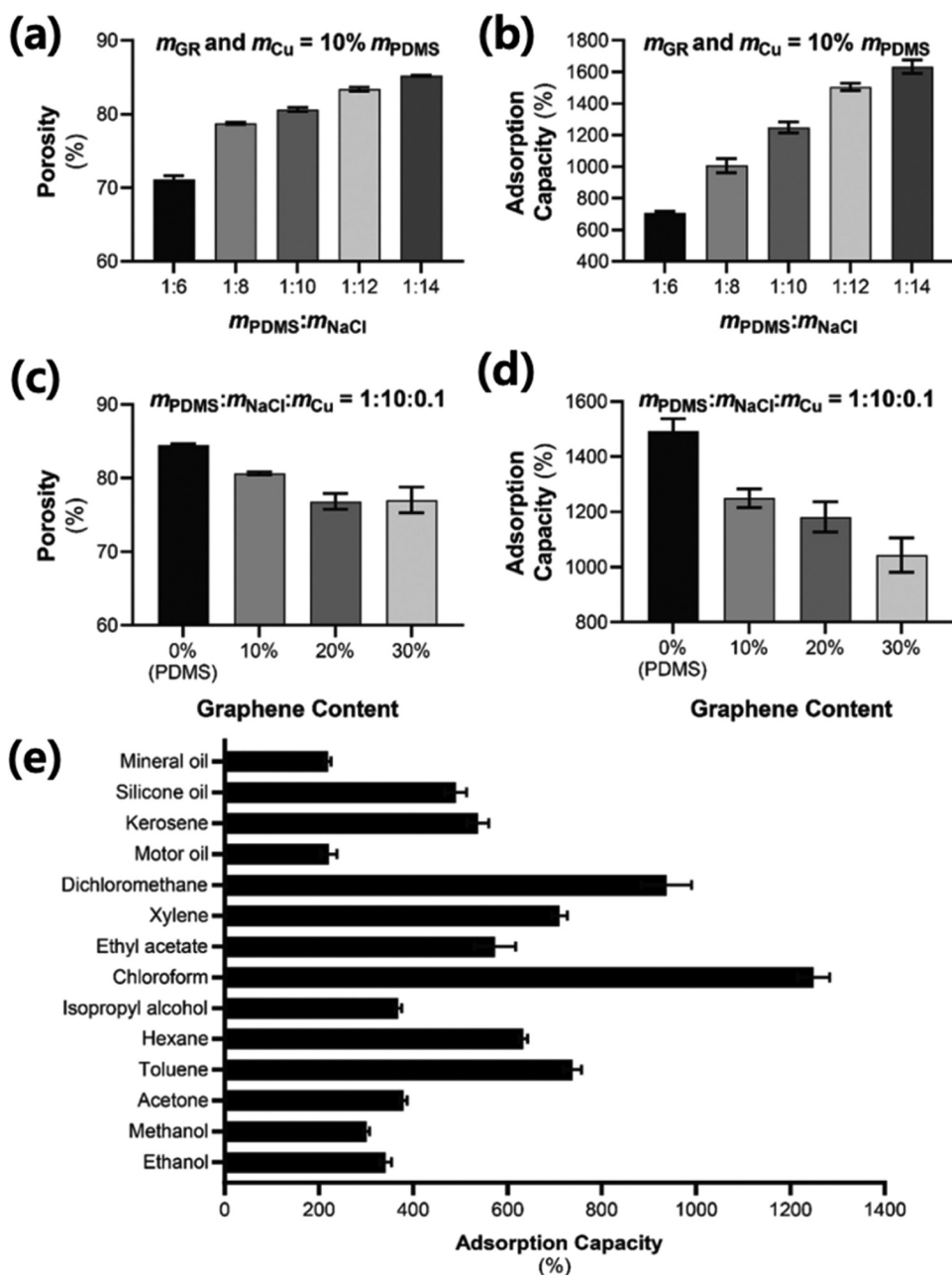


Figure 25. (a, b) porosity and chloroform adsorption capacities of PDMS-GR-Cu foams with different NaCl contents (m_{GR} and $m_{Cu} = 10\% m_{PDMS}$); (c, d) porosity and chloroform adsorption capacity of PDMS-GR-CU foams with different GR contents ($m_{PDMS}/m_{NaCl}/m_{Cu} = 1:10:0.1$). (e) adsorption capacity of the PDMS-GR-Cu foam ($m_{PDMS}/m_{NaCl}/m_{GR}/m_{Cu} = 1:10:0.1:0.1$) toward various oils/organic solvents. Data are shown as mean \pm standard deviation ($n = 5$) (Ozkan et al. 2023). Reprinted with permission from (Ozkan et al. 2023); copyright 2023 American Chemical Society.

reported 14% higher strain values for porous PDMS made with 3D printing compared nonporous PDMS. The mechanical properties, advantages, and disadvantages of each method of fabricating porous PDMS are summarized in Table 1. However, the electrical properties of the PDMS sponge alone are not good enough for its use. In addition, as PDMS becomes a porous structure, its

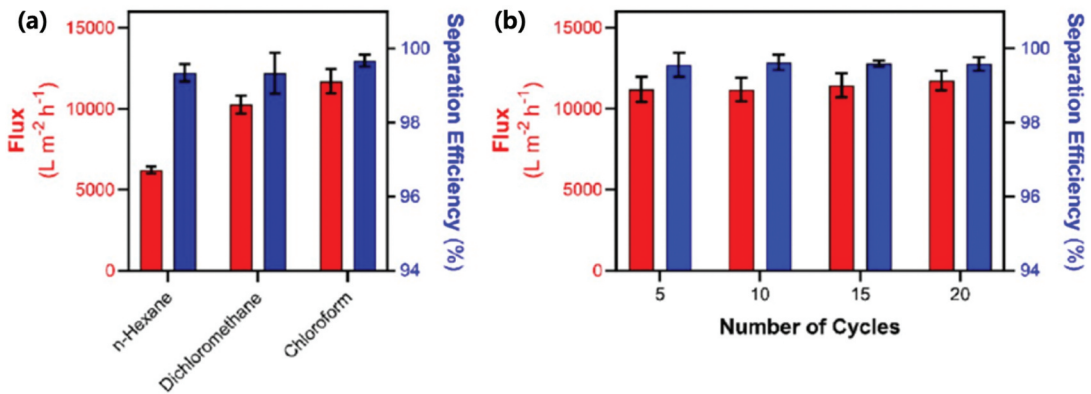


Figure 26. (a) separation efficiency and flux of the PDMS-GR-Cu foam for various oil – water mixtures. (b) separation efficiency and flux of the PDMS-GR-Cu foam with a water – chloroform mixture for different cycles (Ozkan et al. 2023). Reprinted with permission from (Ozkan et al. 2023); copyright 2023 American Chemical Society.

mechanical properties degrade. Therefore, it is difficult to apply to sensors such as microfluidics sensors that require excellent mechanical properties. Therefore, researchers are conducting many studies to improve the electrical conductivity of porous PDMS using various conductive fillers. The improvement of characteristics indicates the possibility of employing PDMS sponge in various applications such as sensors, flexible electrodes, energy harvesting and storage, and oil/water separation. To compensate for the shortcomings,

Song et al. and Jung et al. respectively improved the mechanical stability and electrical conductivity of the PDMS sponge by adding CNT filler to the PDMS sponge and coating it with graphene. Tan et al (Tan and Zheng 2022) obtained a high sensitivity value by coating PDMS using AgNWs as a filler. By coating the NiO/MnO₂/CNT composite with PDMS, Pecenk et al (Peçenek et al. 2022) produced flexible electrodes for use in supercapacitors and obtained excellent performance even after bending several times. Further, Tantraviwat et al (Tantraviwat et al. 2020). and He et al (He et al. 2016) created nanogenerators based on PDMS sponge. The porous PDMS fabricated by Tantraviwat et al. showed higher performance than that of the micropillar and flat pattern. Furthermore, He et al. created flexible nanogenerators using ZnO nanoparticles; it showed high stability and durability even after several cycles. Currently, research is being conducted to apply porous PDMS in various fields such as sensors, nanogenerators, and flexible electrodes. However, further enhancement in properties such as sensitivity and capacity is required to achieve commercialization by using various fillers. For example, PDMS is widely used for microfluidic sensors because of its high stretchability and elasticity, biocompatibility, and transparency. However, in the form of PDMS sponge, their mechanical stability is slightly degraded, which limits their use for microfluidic sensors that require excellent mechanical properties. Therefore, exploring the development of nanocomposites by incorporating materials such as graphene to enhance the mechanical strength of PDMS sponge will hold significant promise for microfluidics sensors. In addition, the low thermal conductivity of PDMS may also pose challenges in the microfluidic sensors where efficient heat transfer is needed. Therefore, a technology to enhance the thermal conductivity will be also required to be developed. Zhao et al (Zhao et al. 2022) developed a sensor with excellent performance by mixing CNT and graphene. Liu et al (Liu et al. 2019) mixed an inorganic substance (Fe₃O₄) and an organic substance (multiwalled CNTs). By utilizing the excellent mechanical properties of CNTs and the high saturation magnetization of Fe₃O₄, a polymer foam with high performance and tunable electromagnetic microwave absorption properties was produced. Thus, the use of two or more substances to compensate for each other's shortcomings and create synergistic effects instead of using only one substance can be suggested. In addition, several studies will be

conducted on fabrication methods such as combining the latest technologies, e.g., 3D printing, to create a porous structure for easier mass production.

Wearable watches have already been commercialized, and more devices will become biocompatible in the future. PDMS, which shows excellent mechanical performance even under high deformation and has excellent thermal stability, is very suitable for use in flexible electrodes and substrates; however, its effect is further increased when creating a nanomaterial composite by making it a porous structure. Porous PDMS, which can be produced with various fabrication methods and combined with various materials to create excellent synergy, will become the most important material in the near future.

Highlights

- Polydimethylsiloxane sponge has various process methods, and materials are used as fillers to obtain desired properties depending on the application.
- Fabrication process of PDMS sponge for each method and mechanical properties are described.
- Applications of PDMS sponge made using fillers such as graphene, CNTs and AgNWs are discussed.

Disclosure statement

No potential conflict of interest was reported by the author(s).

Funding

The work was supported by the National Research Foundation of Korea [2022K1A3A1A39089566]. Project no. 2022-1.2.5-TÉT-IPARI-KR-2022-00013 has been implemented with the support provided by the Ministry of Culture and Innovation of Hungary from the National Research, Development and Innovation Fund, financed under the 2022-1.2.5-TÉT-IPARI-KR funding scheme.

References

- Abshirini, M., M. Cengiz Altan, Y. Liu, M. C. Saha, L. Cummings, and T. Robison. 2020. "Manufacturing of Porous Polydimethylsiloxane (PDMS) Plates Using Solvent Evaporation Induced Phase Separation Technique." *ASME International Mechanical Engineering Congress & Exposition* 24062. <https://doi.org/10.1115/IMECE2020-24062>.
- Abshirini, M., M. C. Saha, M. C. Altan, Y. Liu, L. Cummings, and T. Robison. 2021. "Investigation of Porous Polydimethylsiloxane Structures with Tunable Properties Induced by the Phase Separation Technique." *Journal of Applied Polymer Science* 138 (29): 50688. <https://doi.org/10.1002/app.50688>.
- Abshirini, M., M. C. Saha, M. Cengiz Altan, and Y. Liu. 2021. "Synthesis and Characterization of Hierarchical Porous Structure of Polydimethylsiloxane (PDMS) Sheets via Two-Step Phase Separation Method." *Materials & Design* 212:110194. <https://doi.org/10.1016/j.matdes.2021.110194>.
- Bekyarova, E., S. Sarkar, F. Wang, M. E. Itkis, I. Kalinina, X. Tian, and R. C. Haddon. 2013. "Effect of Covalent Chemistry on the Electronic Structure and Properties of Carbon Nanotubes and Graphene." *Accounts of Chemical Research* 46 (1): 65–76.
- Butt, M. A., N. L. Kazanskiy, and S. N. Khonina. 2022. "Revolution in Flexible Wearable Electronics for Temperature and Pressure Monitoring— a Review." *Electronics* 11 (5): 716.
- Cao, C.-F., P.-H. Wang, J.-W. Zhang, K.-Y. Guo, L. Yang, Q.-Q. Xia, G.-D. Zhang, et al. 2020. "One-Step and Green Synthesis of Lightweight, Mechanically Flexible and Flame-Retardant Polydimethylsiloxane Foam Nanocomposites via Surface-Assembling Ultralow Content of Graphene Derivative." *Chemical Engineering Journal* 393:124724. <https://doi.org/10.1016/j.cej.2020.124724>.
- Cao, C.-F., G.-D. Zhang, Z. Li, L.-X. Gong, J.-F. Gao, J.-X. Jiang, L.-C. Tang, and Y.-W. Mai. 2019. "Design of Mechanically Stable, Electrically Conductive and Highly Hydrophobic Three-Dimensional Graphene Nanoribbon Composites by Modulating the Interconnected Network on Polymer Foam Skeleton." *Composites Science and Technology* 171:162–170. <https://doi.org/10.1016/j.compscitech.2018.12.014>.
- Cui, J., B. Zhang, J. Duan, H. Guo, and J. Tang. 2016. "Flexible Pressure Sensor with Ag Wrinkled Electrodes Based on PDMS Substrate." *Sensors* 16 (12): 2131.
- Dai, S.-W., G. Ya-Li, L. Zhao, W. Zhang, C.-H. Gao, W. Yu-Xi, S.-C. Shen, C. Zhang, T.-T. Kong, and L. Yu-Tong. 2021. "Bamboo-Inspired Mechanically Flexible and Electrically Conductive Polydimethylsiloxane Foam Materials with

- Designed Hierarchical Pore Structures for Ultra-Sensitive and Reliable Piezoresistive Pressure Sensor.” *Composites Part B Engineering* 225:109243. <https://doi.org/10.1016/j.compositesb.2021.109243>.
- Dan, L., S. Shi, H.-J. Chung, and A. Elias. 2019. “Porous Polydimethylsiloxane–Silver Nanowire Devices for Wearable Pressure Sensors.” *Acs Applied Nano Materials* 2 (8): 4869–4878.
- Du, Y., S. Liu, S. Yuan, H. Zhang, and S. Yuan. 2021. “A Study of Influence Factors to Improve the Heat Transfer of Pure-Polydimethylsiloxane (PDMS): A Molecular Dynamics Study.” *Colloids and Surfaces A, Physicochemical and Engineering Aspects* 618:126409. <https://doi.org/10.1016/j.colsurfa.2021.126409>.
- Faraj, M. G., K. Ibrahim, and M. K. M. Ali. 2011. “PET as a Plastic Substrate for the Flexible Optoelectronic Applications.” *Optoelectronics and Advanced Materials – Rapid Communications* 5 (8): 879–882.
- Gandy, P. J. F., S. Bardhan, A. L. Mackay, and J. Klinowski. 2001. “Nodal Surface Approximations to the P,G,D and I-WP Triply Periodic Minimal Surfaces.” *Chemical Physics Letters* 336 (3): 187–195. [https://doi.org/10.1016/S0009-2614\(00\)01418-4](https://doi.org/10.1016/S0009-2614(00)01418-4).
- Gao, J., K. Shang, Y. Ding, and Z. Wen. 2021. “Material and Configuration Design Strategies Towards Flexible and Wearable Power Supply Devices: A Review.” *Journal of Materials Chemistry A* 9 (14): 8950–8965.
- Guo, B.-F., P.-H. Wang, C.-F. Cao, Q. Zhang-Hao, L. Ling-Yu, G.-D. Zhang, L.-X. Gong, P. Song, J.-F. Gao, and Y.-W. Mai. 2022. “Restricted Assembly of Ultralow Loading of Graphene Oxide for Lightweight, Mechanically Flexible and Flame Retardant Polydimethylsiloxane Foam Composites.” *Composites Part B Engineering* 247:110290. <https://doi.org/10.1016/j.compositesb.2022.110290>.
- Ha, H. B., B. H. Lee, N. Qaiser, Y. Seo, J. Kim, J. M. Koo, and B. Hwang. 2022. “Highly Reliable Anisotropic Interconnection System Fabricated Using Cu/sn-Soldered Microdumbbell Arrays and Polyimide Films for Application to Flexible Electronics.” *Intermetallics* 144:107535. <https://doi.org/10.1016/j.intermet.2022.107535>.
- Ha, H., S. Müller, R.-P. Baumann, and B. Hwang n.d. *Peakforce Quantitative Nanomechanical Mapping For Surface Energy Characterization On The Nanoscale: A Mini-review*. Facta Universitatis, Series: Mechanical Engineering. <https://doi.org/10.22190/FUME221126001H>.
- Han, T.-L., B.-F. Guo, G.-D. Zhang, and L.-C. Tang. 2023. “Facile Synthesis of Hollow Glass Microsphere Filled PDMS Foam Composites with Exceptional Lightweight, Mechanical Flexibility, and Thermal Insulating Property.” *Molecules* 28 (6): 2614.
- Ha, H., N. Qaiser, J. H. Jeong, K. Lee, and B. Hwang. 2023. “Highly Stretchable CIP–PDMS Composites with Partial Interface Bonding for Electromagnetic Noise Suppression in GHz Frequency Range.” *Journal of Natural Fibers* 20 (1): 2128149. <https://doi.org/10.1080/15440478.2022.2128149>.
- He, X., X. Mu, Q. Wen, Z. Wen, J. Yang, C. Hu, and H. Shi. 2016. “Flexible and Transparent Triboelectric Nanogenerator Based on High Performance Well-Ordered Porous PDMS Dielectric Film.” *Nano Research* 9:3714–3724. <https://doi.org/10.1007/s12274-016-1242-3>.
- Herren, B., V. Webster, E. Davidson, M. C. Saha, M. Cengiz Altan, and Y. Liu. 2021. “PDMS Sponges with Embedded Carbon Nanotubes as Piezoresistive Sensors for Human Motion Detection.” *Nanomaterials* 11 (7): 1740.
- He, Y., D. Wu, M. Zhou, Y. Zheng, T. Wang, C. Lu, L. Zhang, H. Liu, and C. Liu. 2021. “Wearable Strain Sensors Based on a Porous Polydimethylsiloxane Hybrid with Carbon Nanotubes and Graphene.” *ACS Applied Materials and Interfaces* 13 (13): 15572–15583.
- Huang, L., H. Wang, D. Zhan, and F. Fang. 2021. “Flexible Capacitive Pressure Sensor Based on Laser-Induced Graphene and Polydimethylsiloxane Foam.” *IEEE Sensors Journal* 21 (10): 12048–12056.
- Hu, W. J., Q. Q. Xia, H. T. Pan, H. Y. Chen, Y. X. Qu, Z. Y. Chen, G. D. Zhang, et al. 2022. “Green and Rapid Preparation of Fluorosilicone Rubber Foam Materials with Tunable Chemical Resistance for Efficient Oil– water Separation.” *Polymers* 14 (8): 1628.
- Hwang, B., Y. Han, and P. Matteini. 2022. “BENDING FATIGUE BEHAVIOR of AG NANOWIRE/CU THIN-FILM HYBRID INTERCONNECTS for WEARABLE ELECTRONICS.” 2022:8. <https://doi.org/10.22190/fume220730040h>.
- Jung, Y., K. Jung, B. Park, J. Choi, D. Kim, J. Park, K. Jongsoo, and H. Cho. 2019. “Wearable Piezoresistive Strain Sensor Based on Graphene-Coated Three-Dimensional Micro-Porous PDMS Sponge.” *Micro and Nano Systems Letters* 7 (1): 1–9.
- Jung, Y., W. Lee, K. Jung, B. Park, J. Park, K. Jongsoo, and H. Cho. 2020. “A Highly Sensitive and Flexible Capacitive Pressure Sensor Based on a Porous Three-Dimensional PDMS/Microsphere Composite.” *Polymers* 12 (6): 1412.
- Keller, A., K. Zainulabdeen, H. Warren, and M. In Het Panhuis. 2022. “Fabrication of Porous PDMS Sponges Using Spontaneously Self-Removing Sacrificial Templates.” *MRS Advances* 7 (23–24): 495–498.
- Kim, Y., S. Jang, and O. Je Hoon. 2019. “Fabrication of Highly Sensitive Capacitive Pressure Sensors with Porous PDMS Dielectric Layer via Microwave Treatment.” *Microelectronic Engineering* 215:111002. <https://doi.org/10.1016/j.mee.2019.111002>.
- Kim, S., J. Kim, D. Kim, B. Kim, H. Chae, Y. Hyunjung, and B. Hwang. 2019. “High-Performance Transparent Quantum Dot Light-Emitting Diode with Patchable Transparent Electrodes.” *ACS Applied Materials and Interfaces* 11 (29): 26333–26338. <https://doi.org/10.1021/acsami.9b05969>.
- Kim, W.-G., D.-W. Kim, I.-W. Tcho, J.-K. Kim, M.-S. Kim, and Y.-K. Choi. 2021. “Triboelectric Nanogenerator: Structure, Mechanism, and Applications.” *Agricultural Science & Technology Nano* 15 (1): 258–287.
- Kim, T. K., J. Koo Kim, and O. Chan Jeong. 2011. “Measurement of Nonlinear Mechanical Properties of PDMS Elastomer.” *Microelectronic Engineering* 88 (8): 1982–1985.

- Kim, H., N. Qaiser, and B. Hwang. 2023. "ELECTRO-MECHANICAL RESPONSE of STRETCHABLE PDMS COMPOSITES with a HYBRID FILLER SYSTEM." *Facta Universitatis, Series: Mechanical Engineering* 2023:11. <https://doi.org/10.22190/fume221205002k>.
- Kim, H., N. Qaiser, and B. Hwang. 2023. "Electro-mechanical response of stretchable pdms composites with a hybrid filler system." *Facta Universitatis, Series: Mechanical Engineering* 21 (1): 51–61. <https://doi.org/10.22190/FUME221205002K>.
- Lee, C., H. Kim, and B. Hwang. 2019. "Fracture Behavior of Metal Oxide/Silver Nanowire Composite Electrodes Under Cyclic Bending." *Journal of Alloys and Compounds* 773:361–366. <https://doi.org/10.1016/j.jallcom.2018.09.212>.
- Lee, M., B.-H. Wee, and J.-D. Hong. 2015. "High Performance Flexible Supercapacitor Electrodes Composed of Ultralarge Graphene Sheets and Vanadium Dioxide." *Advanced Energy Materials* 5 (7): 1401890. <https://doi.org/10.1002/aenm.201401890>.
- Lee, H., J. Yoo, J. Park, J. Ho Kim, K. Kang, and Y. Sik Jung. 2012. "A Stretchable Polymer–Carbon Nanotube Composite Electrode for Flexible Lithium-Ion Batteries: Porosity Engineering by Controlled Phase Separation." *Advanced Energy Materials* 2 (8): 976–982.
- Li, S. N., X. F. He, Z. F. Zeng, B. Jiang, Q. Wu, L. X. Gong, Y. Li, J. Bae, S. Wang, and L. C. Tang. 2022. "Mechanically Ductile, Ionically Conductive and Low-Temperature Tolerant Hydrogel Enabled by High-Concentration Saline Towards Flexible Strain Sensor." *Nano Energy* 103:107789. <https://doi.org/10.1016/j.nanoen.2022.107789>.
- Li, X. P., Y. Li, X. Li, D. Song, P. Min, C. Hu, H. B. Zhang, N. Koratkar, and Z. Z. Yu. 2019. "Highly Sensitive, Reliable and Flexible Piezoresistive Pressure Sensors Featuring Polyurethane Sponge Coated with MXene Sheets." *Journal of Colloid and Interface Science* 542:54–62.
- Li, B., J. Luo, X. Huang, L. Lin, L. Wang, M. Hu, L. Tang, H. Xue, J. Gao, and Y. W. Mai. 2020. "A Highly Stretchable, Super-Hydrophobic Strain Sensor Based on Polydopamine and Graphene Reinforced Nanofiber Composite for Human Motion Monitoring." *Composites Part B Engineering* 181:107580. <https://doi.org/10.1016/j.compositesb.2019.107580>.
- Liu, C., Y. Duan, J. Cai, L. Xinghao, D. Zhang, J. Gao, and Y. Che. 2019. "Compressible Fe₃O₄/MWCNTs-Coated Polymer Foams for High-Performance and Tunable Electromagnetic Microwave Absorption." *Materials Research Express* 6 (10): 106114. <https://doi.org/10.1088/2053-1591/ab3a05>.
- Li, S. N., Z. R. Yu, B. F. Guo, K. Y. Guo, Y. Li, L. X. Gong, L. Zhao, J. Bae, and L. C. Tang. 2021. "Environmentally Stable, Mechanically Flexible, Self-Adhesive, and Electrically Conductive Ti₃C₂TX MXene Hydrogels for Wide-Temperature Strain Sensing." *Nano Energy* 90:106502. <https://doi.org/10.1016/j.nanoen.2021.106502>.
- Long, Y., X. Zhao, X. Jiang, L. Zhang, H. Zhang, Y. Liu, and H. Zhu. 2018. "A Porous Graphene/Polydimethylsiloxane Composite by Chemical Foaming for Simultaneous Tensile and Compressive Strain Sensing." *FlatChem* 10:1–7. <https://doi.org/10.1016/j.flatc.2018.07.001>.
- Lu, S. Y., M. Jin, Y. Zhang, Y. B. Niu, J. C. Gao, and C. Li. 2018. "Chemically Exfoliating Biomass into a Graphene-Like Porous Active Carbon with Rational Pore Structure, Good Conductivity, and Large Surface Area for High-Performance Supercapacitors." *Advanced Energy Materials* 8 (11): 1702545 doi:<https://doi.org/10.1002/aenm.201702545>.
- Lu, Y., Y. Mi, T. Wu, X. Cao, and N. Wang. 2022. "From Triboelectric Nanogenerator to Polymer-Based Biosensor: A Review." *Biosensors* 12 (5): 323.
- Luo, W., M. Charara, M. C. Saha, and Y. Liu. 2019. "Fabrication and Characterization of Porous CNF/PDMS Nanocomposites for Sensing Applications." *Applied Nanoscience* 9:1309–1317. <https://doi.org/10.1007/s13204-019-00958-x>.
- Lv, L. Y., C. F. Cao, Y. X. Qu, G. D. Zhang, L. Zhao, K. Cao, P. Song, and L. C. Tang. 2022. "Smart Fire-Warning Materials and Sensors: Design Principle, Performances, and Applications." *Materials Science and Engineering: R: Reports* 150:100690. <https://doi.org/10.1016/j.msere.2022.100690>.
- Montazerian, H., M. G. A. Mohamed, M. Mohaghegh Montazeri, S. Kheiri, A. S. Milani, K. Kim, and M. Hoorfar. 2019. "Permeability and Mechanical Properties of Gradient Porous PDMS Scaffolds Fabricated by 3D-Printed Sacrificial Templates Designed with Minimal Surfaces." *Acta Biomaterialia* 96:149–160. <https://doi.org/10.1016/j.actbio.2019.06.040>.
- Oropallo, W., and L. A. Piegl. 2016. "Ten Challenges in 3D Printing." *Engineering with Computers* 32:135–148. <https://doi.org/10.1007/s00366-015-0407-0>.
- Ozkan, E., M. Garren, J. Manuel, M. Douglass, R. Devine, A. Mondal, A. Kumar, M. Ashcraft, R. Pandey, and H. Handa. 2023. "Superhydrophobic and Conductive Foams with Antifouling and Oil–Water Separation Properties." *ACS Applied Materials and Interfaces* 15 (5): 7610–7626.
- Paghi, A., M. Corsi, S. Corso, S. Mariani, and G. Barillaro. 2022. "In situ Controlled and Conformal Coating of Polydimethylsiloxane Foams with Silver Nanoparticle Networks with Tunable Piezo-Resistive Properties." *Nanoscale Horizons* 7 (4): 425–436.
- Pan, P., Z. Bian, X. Song, and X. Zhou. 2020. "Properties of Porous PDMS and Stretchability of Flexible Electronics in Moist Environment." *Journal of Applied Mechanics* 87 (10): 101009. <https://doi.org/10.1115/1.4047775>

- Pan, Z., Y. Guan, Y. Liu, and F. Cheng. 2021. "Facile Fabrication of Hydrophobic and Underwater Superoleophilic Elastic and Mechanical Robust Graphene/PDMS Sponge for Oil/Water Separation." *Separation and Purification Technology* 261:118273. <https://doi.org/10.1016/j.seppur.2020.118273>.
- Peçenek, H., M. S. O. Fatma Kılıç Dokan, E. Yılmaz, and E. Sahmetlioglu. 2022. "Highly Compressible Binder-Free Sponge Supercapacitor Electrode Based on Flower-Like NiO/MnO₂/CNT." *Journal of Alloys and Compounds* 913:165053. <https://doi.org/10.1016/j.jallcom.2022.165053>.
- Peng, H., J. Huang, M. Zhao, Q. Zhang, X. Cheng, X. Liu, W. Qian, and F. Wei. 2014. "Nanoarchitected Graphene/CNT@ Porous Carbon with Extraordinary Electrical Conductivity and Interconnected Micro/Mesopores for Lithium-Sulfur Batteries." *Advanced Functional Materials* 24 (19): 2772–2781. <https://doi.org/10.1002/adfm.201303296>.
- Pharino, U., Y. Sinsanong, S. Pongampai, T. Charoonsuk, P. Pakawanit, S. Sriphan, N. Vittayakorn, and W. Vittayakorn. 2021. "Influence of Pore Morphologies on the Mechanical and Tribo-Electrical Performance of Polydimethylsiloxane Sponge Fabricated via Commercial Seasoning Templates." *Radiation Physics & Chemistry* 189:109720. <https://doi.org/10.1016/j.radphyschem.2021.109720>.
- Pruvost, M., W. J. Smit, C. Monteux, P. Poulin, and A. Colin. 2019. "Polymeric Foams for Flexible and Highly Sensitive Low-Pressure Capacitive Sensors." *Npj Flexible Electronics* 3 (1): 7. <https://doi.org/10.1038/s41528-019-0052-6>.
- Qiang, F., S.-W. Dai, Z. Li, L.-X. Gong, G.-D. Zhang, J.-X. Jiang, and L.-C. Tang. 2019. "An Insulating Second Filler Tuning Porous Conductive Composites for Highly Sensitive and Fast Responsive Organic Vapor Sensor." *Sensors and Actuators B, Chemical* 285:254–263. <https://doi.org/10.1016/j.snb.2019.01.043>.
- Seo, Y., K. Seongchan, H. Heebo, N. Qaiser, M. Leem, S. Jo Yoo, J. Hyeon Jeong, K. Lee, and B. Hwang. 2022. "Stretchable Carbonyl Iron Powder/Polydimethylsiloxane Composites for Noise Suppression in Gigahertz Bandwidth." *Composites Science and Technology* 218:109150. <https://doi.org/10.1016/j.compscitech.2021.109150>.
- Shieh, J.-Y., S.-Y. Tsai, L. Bo-Yan, and Y. Hsin Her. 2017. "High-Performance Flexible Supercapacitor Based on Porous Array Electrodes." *Materials Chemistry and Physics* 195:114–122. <https://doi.org/10.1016/j.matchemphys.2017.04.034>.
- Song, Y., H. Chen, S. Zongming, X. Chen, L. Miao, J. Zhang, X. Cheng, and H. Zhang. 2017. "Highly Compressible Integrated Supercapacitor–Piezoresistance-sensor System with CNT–PDMS Sponge for Health Monitoring." *Small* 13 (39): 1702091. <https://doi.org/10.1002/sml.201702091>.
- Song, W.-J., S. Lee, G. Song, H. Bin Son, D.-Y. Han, I. Jeong, Y. Bang, and S. Park. 2020. "Recent Progress in Aqueous Based Flexible Energy Storage Devices." *Energy Storage Materials* 30:260–286. <https://doi.org/10.1016/j.ensm.2020.05.006>.
- Stoller, M. D., C. W. Magnuson, Y. Zhu, S. Murali, J. Won Suk, R. Piner, and R. S. Ruoff. 2011. "Interfacial Capacitance of Single Layer Graphene." *Energy & Environmental Science* 4 (11): 4685–4689.
- Sun, X., J. Sun, L. Tong, S. Zheng, C. Wang, W. Tan, J. Zhang, C. Liu, M. Tianjun, and Q. Zhimei. 2019. "Flexible Tactile Electronic Skin Sensor with 3D Force Detection Based on Porous CNTs/PDMS Nanocomposites." *Nano-Micro Letters* 11:1–14. <https://doi.org/10.1007/s40820-019-0288-7>.
- Szalai, S., S. S. Kocsis, D. Harangozó, and S. Fischer. 2022. "Investigation of Deformations of a Lithium Polymer Cell Using the Digital Image Correlation Method (DICM)." *Reports in Mechanical Engineering* 3 (2): 206–224. <https://doi.org/10.31181/rme20008022022s>.
- Tantraviwat, D., P. Buarin, S. Suintalelat, W. Sripumkhai, P. Pattamang, G. Rujijanagul, and B. Inceesungvorn. 2020. "Highly Dispersed Porous Polydimethylsiloxane for Boosting Power-Generating Performance of Triboelectric Nanogenerators." *Nano Energy* 67:104214. <https://doi.org/10.1016/j.nanoen.2019.104214>.
- Tan, X., and J. Zheng. 2022. "A Novel Porous PDMS-AgNWs-PDMS (PAP)-Sponge-Based Capacitive Pressure Sensor." *Polymers* 14 (8): 1495. <https://doi.org/10.3390/polym14081495>.
- Turco, A., A. Grazia Monteduro, F. Montagna, E. Primiceri, M. Frigione, and G. Maruccio. 2023. "The Effect of Synthetic Conditions on Piezoresistive Properties of Ultrasensitive Carbon Nanotube/PDMS 3D Composites." *Polymer* 264:125534. <https://doi.org/10.1016/j.polymer.2022.125534>.
- Turco, A., E. Primiceri, M. Frigione, G. Maruccio, and C. Malitesta. 2017. "An Innovative, Fast and Facile Soft-Template Approach for the Fabrication of Porous PDMS for Oil–Water Separation." *Journal of Materials Chemistry A* 5 (45): 23785–23793.
- Ulbricht, M. 2006. "Advanced Functional Polymer Membranes." *Polymer* 47 (7): 2217–2262.
- Wang, H., M. Han, Y. Song, and H. Zhang. 2021. "Design, Manufacturing and Applications of Wearable Triboelectric Nanogenerators." *Nano Energy* 81:105627. <https://doi.org/10.1016/j.nanoen.2020.105627>.
- Wang, D., H. Liu, F. Liu, M. Guorong, J. Yang, G. Xiaodan, M. Zhou, and Z. Chen. 2021. "Phase-Separation-Induced Porous Lithiophilic Polymer Coating for High-Efficiency Lithium Metal Batteries." *Nano Letters* 21 (11): 4757–4764.
- Wang, C., P. Wang, J. Chen, L. Zhu, D. Zhang, Y. Wan, and A. Shiyun. 2022. "Self-Powered Biosensing System Driven by Triboelectric Nanogenerator for Specific Detection of Gram-Positive Bacteria." *Nano Energy* 93:106828. <https://doi.org/10.1016/j.nanoen.2021.106828>.
- Woo, R., G. Chen, J. Zhao, and J. Bae. 2021. "Structure–Mechanical Property Relationships of 3D-Printed Porous Polydimethylsiloxane." *ACS Applied Polymer Materials* 3 (7): 3496–3503. <https://doi.org/10.1021/acsapm.1c00417>.

- Wu, X., Y. Han, X. Zhang, Z. Zhou, and C. Lu. 2016. "Large-Area Compliant, Low-Cost, and Versatile Pressure-Sensing Platform Based on Microcrack-Designed Carbon Black@ Polyurethane Sponge for Human–Machine Interfacing." *Advanced Functional Materials* 26 (34): 6246–6256.
- Yang, Z., W. Zijian, D. Jiang, R. Wei, X. Mai, D. Pan, S. Vupputuri, L. Weng, N. Naik, and Z. Guo. 2021. "Ultra-Sensitive Flexible Sandwich Structural Strain Sensors Based on a Silver Nanowire Supported PDMS/PVDF Electrospun Membrane Substrate." *Journal of Materials Chemistry C* 9 (8): 2752–2762. <https://doi.org/10.1039/D0TC04659K>.
- Yu, C., C. Yu, L. Cui, Z. Song, X. Zhao, Y. Ma, and L. Jiang. 2017. "Facile Preparation of the Porous PDMS Oil-Absorbent for Oil/Water Separation." *Advanced Materials Interfaces* 4 (3): 1600862. <https://doi.org/10.1002/admi.201600862>
- Zhang, S., M. Bick, X. Xiao, G. Chen, A. Nashalian, and J. Chen. 2021. "Leveraging Triboelectric Nanogenerators for Bioengineering." *Matter* 4 (3): 845–887. <https://doi.org/10.1016/j.matt.2021.01.006>.
- Zhang, W., H. Cheng, Q. Niu, F. Mingli, H. Huang, and Y. Daiqi. 2019. "Microbial Targeted Degradation Pretreatment: A Novel Approach to Preparation of Activated Carbon with Specific Hierarchical Porous Structures, High Surface Areas, and Satisfactory Toluene Adsorption Performance." *Environmental Science & Technology* 53 (13): 7632–7640. <https://doi.org/10.1021/acs.est.9b01159>.
- Zhang, G.-D., W. Zhi-Hao, Q.-Q. Xia, Q. Yong-Xiang, H.-T. Pan, H. Wan-Jun, L. Zhao, K. Cao, E.-Y. Chen, and Z. Yuan. 2021. "Ultrafast Flame-Induced Pyrolysis of Poly (Dimethylsiloxane) Foam Materials Toward Exceptional Superhydrophobic Surfaces and Reliable Mechanical Robustness." *ACS Applied Materials and Interfaces* 13 (19): 23161–23172. <https://doi.org/10.1021/acsami.1c03272>.
- Zhao, Y., X. Lei, X. Jiandong, L. Yunfan, W. Weiguang, X. Guo, T. Ren, and F. Liu. 2022. "High-Performance Porous PDMS-Based Piezoresistive Sensor Prepared by a Modified Microwave Irradiation Process." *ACS Applied Electronic Materials* 4 (11): 5498–5505. <https://doi.org/10.1021/acsaelm.2c01123>.
- Zhao, L., F. Qiang, S.-W. Dai, S.-C. Shen, Y.-Z. Huang, N.-J. Huang, G.-D. Zhang, L.-Z. Guan, J.-F. Gao, and Y.-H. Song. 2019. "Construction of Sandwich-Like Porous Structure of Graphene-Coated Foam Composites for Ultrasensitive and Flexible Pressure Sensors." *Nanoscale* 11 (21): 10229–10238. <https://doi.org/10.1039/C9NR02672J>.
- Zhong, W., X. Ding, L. Weixin, C. Shen, A. Yadav, Y. Chen, M. Bao, H. Jiang, and D. Wang. 2019. "Facile Fabrication of Conductive Graphene/Polyurethane Foam Composite and Its Application on Flexible Piezo-Resistive Sensors." *Polymers* 11 (8): 1289. <https://doi.org/10.3390/polym11081289>.
- Zhou, L., J. Rada, H. Zhang, H. Song, S. Mirniaharikandi, B. S. Ooi, and Q. Gan. 2021. "Sustainable and Inexpensive Polydimethylsiloxane Sponges for Daytime Radiative Cooling." *Advanced Science* 8 (23): 2102502. <https://doi.org/10.1002/advs.202102502>.
- Zhu, D., S. Handschuh-Wang, and X. Zhou. 2017. "Recent Progress in Fabrication and Application of Polydimethylsiloxane Sponges." *Journal of Materials Chemistry A* 5 (32): 16467–16497. <https://doi.org/10.1039/C7TA04577H>.